

Innovative stainless-steel connector for double-tee girders under various loading conditions

by

Trevor Young

B.S., Kansas State University, 2020

A THESIS

submitted in partial fulfillment of the requirements for the degree

MASTER OF SCIENCE

Department of Civil Engineering
Carl R. Ice College of Engineering

KANSAS STATE UNIVERSITY
Manhattan, Kansas

2021

Approved by:

Major Professor
Hayder A. Rasheed

Copyright

© Trevor Young 2021.

Abstract

Steel connections embedded in the flanges of precast double-tee concrete girders are a common type of connection to join precast elements together to create floor diaphragm systems in structures such as parking garages. These steel connections are the main load transferring elements in precast structures and have been observed to be inadequate needing repairs after being in service due to high load demands. The main objective of this research was to evaluate the strength of a newly designed stainless-steel connector as a repair solution for failing embedded connections in preexisting precast structures. The connectors were embedded into the edges of concrete prototype slabs to simulate the behavior of the connector when it was embedded into the sides of the flanges of precast double-tee concrete girders. An experimental program was developed to determine the load capacity of the connector and its embedment as deformation occurred. The procedure involved monotonic tests for axial tension, horizontal shear, and vertical shear followed by cyclic tests for horizontal shear and vertical shear. In addition, a flexural capacity test was performed on two slabs adjoined by the proposed connector. Very promising results are generated indicating a superior behavior for this connector compared to the state-of-the-art detail. The observed experimental capacities of the connectors are paired with some analytical models to support the overall strength development determined for the connectors.

Table of Contents

List of Figures	vi
List of Tables	xii
Chapter 1 - Introduction.....	1
Chapter 2 - Literature Review.....	4
Chapter 3 - Material Properties.....	10
Chapter 4 - Connector Installation.....	11
Chapter 5 - Experimental Program	14
Monotonic Loading.....	18
Axial Tension Test.....	18
Monotonic Horizontal Shear Test.....	21
Monotonic Vertical Shear Test	24
Cyclic Loading.....	28
Cyclic Horizontal Shear Test.....	28
Cyclic Vertical Shear Test	29
Flexural Test	31
Chapter 6 - Results and Discussions.....	40
Monotonic Loading.....	41
Axial Tension Test.....	41
Monotonic Horizontal Shear Test.....	47
Monotonic Vertical Shear Test	53
Cyclic Loading.....	58
Cyclic Horizontal Shear Test	58

Cyclic Vertical Shear Test	64
Flexural Test	74
Chapter 7 - Modeling and Design Equations	80
Axial Tension Model	80
Vertical Shear Model	83
Horizontal Shear Model	87
Flexural Model	89
Chapter 8 - Conclusions and Recommendations	94
References	97

List of Figures

Figure 1.1. V-Wrap Stainless-Steel Shear Connector.....	2
Figure 1.2. Typical slab reinforcement.....	2
Figure 2.1. Hairpin connector	5
Figure 2.2. Stud-welded and plate connector.....	5
Figure 2.3. Structural tee connector.....	5
Figure 2.4. Bent wing connector.....	5
Figure 4.1. Typical connectors prepared for embedment	11
Figure 4.2. Typical slot cut in a slab.....	12
Figure 4.3. Final mixing of the epoxy.....	12
Figure 4.4. Application of epoxy putty	13
Figure 4.5. Connector after installation	13
Figure 5.1. Actuator fixturing.....	15
Figure 5.2. Steel table	15
Figure 5.3. Steel tube filled with concrete	15
Figure 5.4. Test fixture components	17
Figure 5.5. MTS data acquisition system sample output screen.....	18
Figure 5.6. Axial tension applied load direction.....	19
Figure 5.7. Axial tension test fixities.....	20
Figure 5.8. Axial tension test fixture	21
Figure 5.9. Axial tension string potentiometer placement.....	21
Figure 5.10: Horizontal shear applied load direction.....	22
Figure 5.11. Horizontal shear table and slab orientation	23

Figure 5.12. Horizontal shear slab fixturing	23
Figure 5.13. Horizontal shear test fixture	24
Figure 5.14. Horizontal shear string potentiometer placement.....	24
Figure 5.15. Vertical shear applied load	25
Figure 5.16. Vertical shear slab orientation	25
Figure 5.17. Vertical shear table and slab fixturing.....	25
Figure 5.18. Vertical shear slab alignment and string potentiometer placement.....	26
Figure 5.19. Vertical shear test fixture.....	27
Figure 5.20. Vertical shear test fixture (side view).....	27
Figure 5.21. Cyclic horizontal shear loading.....	29
Figure 5.22. Cyclic vertical shear loading	30
Figure 5.23. Cyclic vertical shear test fixture	30
Figure 5.24. Cyclic vertical shear test fixture.....	30
Figure 5.25. Flexural test setup.....	31
Figure 5.26. Flexural test connector prepared for installation.....	32
Figure 5.27. Flexural test cantilevered slab	33
Figure 5.28. Aligned slots for the flexural test	33
Figure 5.29. Slabs fixed to the tables for the flexural test	34
Figure 5.30. Slab overhang on the tables.....	34
Figure 5.31. Connector installation for the flexural test	35
Figure 5.32. Connector inserted below the top face of the slabs	35
Figure 5.33. Installed connector for the flexural test.....	36
Figure 5.34. Flexural test applied load location.....	38

Figure 5.35. Flexural test fixture.....	38
Figure 5.36. Roller over the embedded connector.....	39
Figure 5.37. Roller located over the steel table	39
Figure 5.38. Flexural test string potentiometer placement	39
Figure 5.39. Actuator test fixture.....	39
Figure 6.1. Axial tension tests force versus actuator displacement plot.....	42
Figure 6.2. Axial tension tests force versus string potentiometer displacement plot	42
Figure 6.3. S1C1 top slab face cracking	43
Figure 6.4. S1C1 bottom slab face cracking.....	43
Figure 6.5. S2C4 top slab face cracking	44
Figure 6.6. S2C4 bottom slab face cracking.....	44
Figure 6.7. S3C7 after the epoxy slipping from around the connector.....	45
Figure 6.8. S3C7 No visible cracking after testing.....	46
Figure 6.9. S4C10 concrete cracking in tension	47
Figure 6.10. Horizontal shear tests force versus actuator displacement plot.....	49
Figure 6.11. Horizontal shear tests force versus string potentiometer displacement	50
Figure 6.12. S1C3 cracking away from the connector.....	51
Figure 6.13. Typical connector-epoxy separation.....	51
Figure 6.14. Typical start of permanent deformation of the connector	52
Figure 6.15. Typical connector rotation around 6,000 lbf.....	52
Figure 6.16. Typical crushing of concrete under the connector	52
Figure 6.17. Vertical shear tests force versus actuator displacement	54
Figure 6.18. Vertical shear tests force versus string potentiometer displacement.....	54

Figure 6.19. S6C15 cracking at the end of the test	55
Figure 6.20. S6C15 concrete cracked under the embedment.....	56
Figure 6.21. S7C17 cracking at failure	56
Figure 6.22. S6C16 cracking at failure	56
Figure 6.23. S7C17 cracking at failure	56
Figure 6.24. Typical large gaps in the cracks after failure for vertical shear tests	57
Figure 6.25. S5C14 force versus actuator displacement plot.....	60
Figure 6.26. S5C14 force versus string potentiometer displacement plot	60
Figure 6.27. S8C19 force versus actuator displacement plot.....	61
Figure 6.28. S8C19 force versus string potentiometer displacement plot	61
Figure 6.29. S8C20 force versus actuator displacement plot.....	62
Figure 6.30. S8C20 force versus string potentiometer displacement plot	62
Figure 6.31. Typical cyclic horizontal shear connector with an applied load	64
Figure 6.32. Typical cyclic horizontal shear connector permanently deformed after testing.....	64
Figure 6.33. S3C8 force versus actuator displacement plot.....	66
Figure 6.34. S3C8 force versus string potentiometer displacement plot	66
Figure 6.35. S3C9 force versus actuator displacement plot.....	67
Figure 6.36. S3C9 force versus string potentiometer displacement plot	67
Figure 6.37. S4C11 force versus actuator displacement plot.....	68
Figure 6.38. S4C11 force versus string potentiometer displacement plot	68
Figure 6.39. S4C12 force versus actuator displacement plot.....	69
Figure 6.40. S4C12 force versus string potentiometer displacement plot	69
Figure 6.41. S3C9 failure.....	70

Figure 6.42. S4C11 failure.....	70
Figure 6.43. S4C12 failure.....	70
Figure 6.44. S3C8 failure on the bottom face.....	71
Figure 6.45. S3C8 failure (slab edge view)	71
Figure 6.46. S3C9 separated connector	72
Figure 6.47. S3C9 debonded epoxy.....	72
Figure 6.48. S4C11 separated connector	73
Figure 6.49. S4C11 spalled embedment and exposed wire mesh rebar.....	73
Figure 6.50. Flexure test force versus string potentiometer displacement	75
Figure 6.51. S9 cracked at yielding	77
Figure 6.52. S8 cracked at ultimate yielding	77
Figure 6.53. Slab rotations after flexural test.....	77
Figure 6.54. Top view of the slabs after the flexural test	78
Figure 6.55. S9 face and edge cracks.....	79
Figure 6.56. S8 face and edge cracks.....	79
Figure 6.57. Embedment crack after the flexural test.....	79
Figure 7.1. Axial tension model diagram.....	81
Figure 7.2. Vertical shear model side view diagram	83
Figure 7.3. Vertical shear model top view diagram.....	84
Figure 7.4. Horizontal Shear Model: Secant stiffness moment-curvature plot.....	88
Figure 7.5. Horizontal shear model force versus displacement plot.....	88
Figure 7.6. Flexural model plastic hinge location.....	90
Figure 7.7. Half-width analysis detailing.....	90

Figure 7.8. Tapered analysis side view detailing	90
Figure 7.9. Tapered analysis top view detailing	91
Figure 7.10. Flexural model load versus displacement plot	92

List of Tables

Table 3.1. Concrete Properties.....	10
Table 3.2. Stainless-Steel Properties.....	10
Table 6.1. Axial tension test results.....	41
Table 6.2. Horizontal shear linear-elastic region.....	48
Table 6.3. Horizontal shear at the start of strain hardening region.....	48
Table 6.4. Horizontal shear at the beginning of ultimate yield region.....	49
Table 6.5. Vertical shear test results.....	53
Table 6.6. Monotonic and cyclic horizontal shear linear-elastic deformation.....	59
Table 6.7. Monotonic and cyclic horizontal shear at the start of strain hardening region.....	59
Table 6.8. Monotonic and cyclic vertical shear test results.....	65
Table 6.9. Flexural test results.....	74
Table 7.1. General Parameters for the Axial Tension Model.....	81
Table 7.2. Axial Tension Model Results.....	83
Table 7.3. General parameters for the vertical shear model.....	84
Table 7.4. Vertical shear model results.....	86
Table 7.5. First plastic hinge loads and displacements.....	92
Table 7.6. Second plastic hinge loads and displacements.....	93
Table 7.7. Third plastic hinge loads and displacements.....	93
Table 8.1. Strength Capacity of the V-Wrap Stainless-Steel Shear connector.....	95

Chapter 1 - Introduction

The repair of steel embed connections in precast concrete systems is a time-consuming and therefore costly process that is not a permanent solution for the structural integrity and overall lifespan of the system. This paper summarizes the findings on a newly designed innovative stainless-steel connector as a repair solution for failing steel embed connections in precast concrete elements. The proposed solution was V-Wrap Stainless-Steel Shear Connectors, provided by Structural Technologies Inc. The objective of this research was to experimentally evaluate the strength of repaired elements when the connector was under various load conditions. The V-Wrap Shear Connector was embedded in concrete slabs to simulate the behavior of this connector when embedded into the sides of the flanges of precast double-tee concrete girders.

The connectors were composed of 3/16-inch thick T316 Stainless-Steel (UNS S31600) and were trapezoidal in shape with a top length of 15 inches, a bottom length of 6 inches, and a height of 3 inches, see Figure 1.1. The concrete slabs that the connectors were embedded in were 48"x48"x4" normal-weight reinforced concrete. The reinforcement in the slabs was 6"x6" wire mesh and two #4 bars that cross diagonally across opposite corners of the slabs with hooked ends, see Figure 1.2. This slab detail is similar to a previous research study from Shaikh and Feile (2004). An additional section of rebar was bent and tied to the slab reinforcement to create a lifting hook on the top face of the slab. The connectors were not cast into the slabs for their embedment but were installed after the slabs had cured. The installation process of the connectors into the slabs followed a procedure for how they would be embedded to repair pre-existing concrete structures. This procedure required the specimens to be prepared with tools and equipment that would be available to construction workers on a job site and not in a lab setting. Epoxy resin was chosen as the material to conjoin the connectors to the slabs.

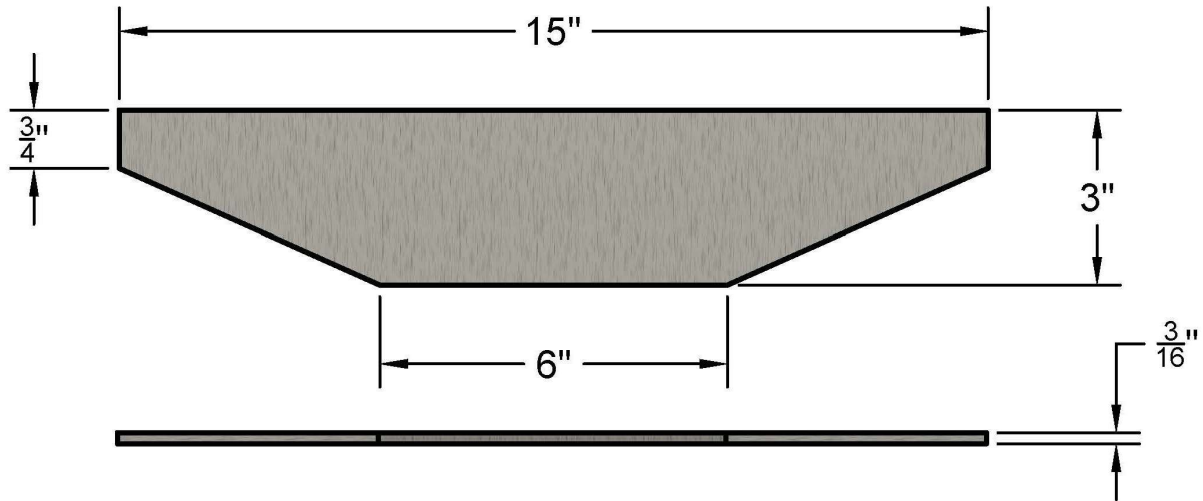


Figure 1.1. V-Wrap Stainless-Steel Shear Connector

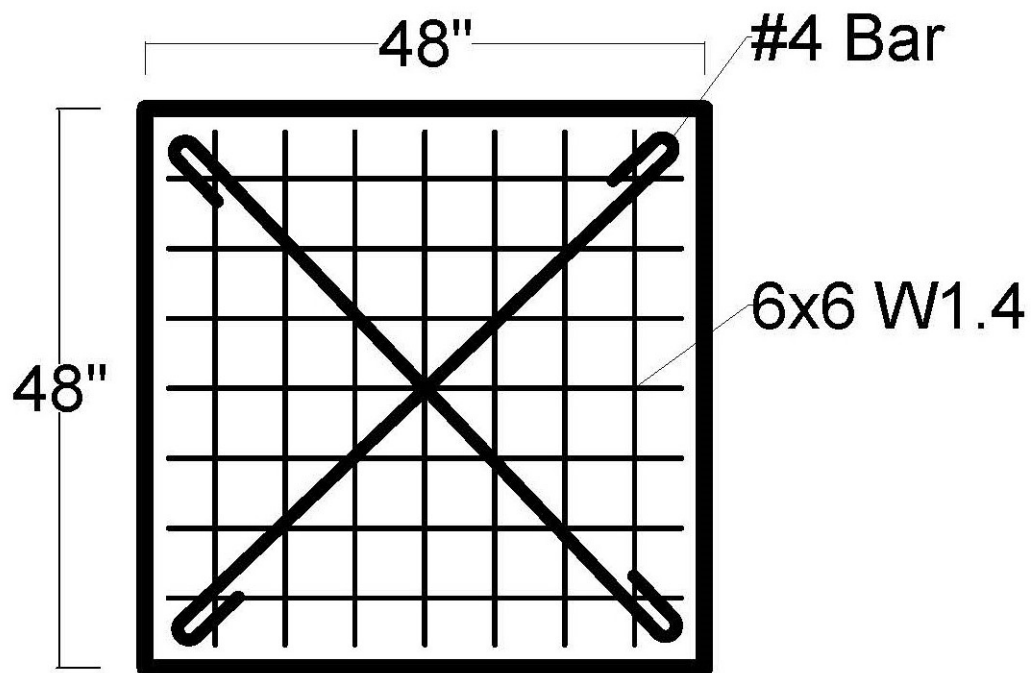


Figure 1.2. Typical slab reinforcement

The experimental program developed for this research used three types of loading protocols to evaluate the responses of the connectors. The protocols were monotonic loading, cyclic loading, and flexural loading of the connectors. Six total types of tests were conducted with these various protocols. There were three types of monotonic loading tests that were

conducted for axial tension, horizontal shear, and vertical shear responses of the connectors. The cyclic loading protocol repeated the horizontal shear and vertical shear tests. The flexural test used a monotonic load rate and was conducted on two cantilevered slabs adjoined by a connector. A total of twenty (20) connectors were tested for this research. Twelve (12) connectors were tested monotonically: four (4) in axial tension, four (4) in horizontal shear, and four (4) in vertical shear. Seven (7) connectors were tested cyclically: three (3) in horizontal shear and four (4) in vertical shear. One flexural test was conducted.

The data and observations gathered from these tests was used to support the development of analytical models. Four models were developed for axial tension, horizontal shear, vertical shear, and flexural capacity. The analytical models use the interaction of the connector and its embedment in the concrete to predict strength capacities and possible failure modes.

Chapter 2 - Literature Review

Mechanical steel connections are a common way to quickly construct precast concrete structures as opposed to topping the elements with a poured diaphragm. A typical example of mechanical connectors can be found in flange-to-flange connections in parking garage structures that use precast double-tee concrete girders to create a diaphragm system. Steel connectors can vary in size and geometric composition for anchoring the connector in the concrete element. Some examples of commonly used connections are presented in Figure 2.1, Figure 2.2, Figure 2.3, and Figure 2.4. The connectors are cast into place in newly constructed precast elements and are field welded together on construction sites. The strength of the connections began to be experimentally evaluated shortly after the 1994 Northridge earthquake event. Experiments conducted for in-plane, or horizontal shear, forces are designed to mimic lateral loads encountered in diaphragm systems. Out-of-plane, or vertical shear, forces replicate loadings from cars or other loads acting in the direction of gravity. Both types of shear forces are used to analyze the responses of the mechanical connectors during seismic events. In-plane tension forces are experimentally tested to assess the bending capacity at the connectors joint under lateral loading of wind and seismic effects. Analytical research has been developed with the increase of experimental research to provide further understanding of stresses and failure modes of connections in diaphragms.

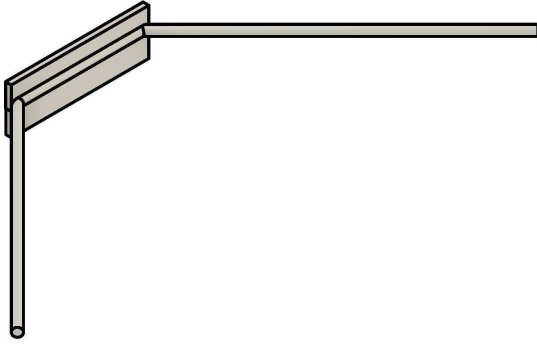


Figure 2.1. Hairpin connector

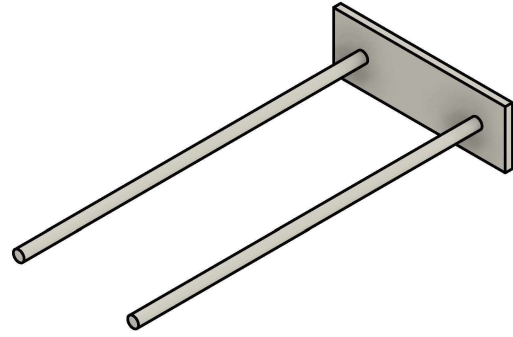


Figure 2.2. Stud-welded and plate connector

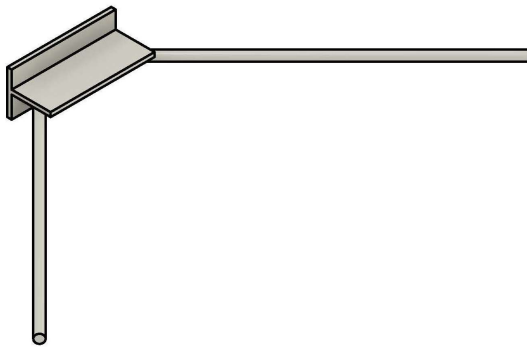


Figure 2.3. Structural tee connector

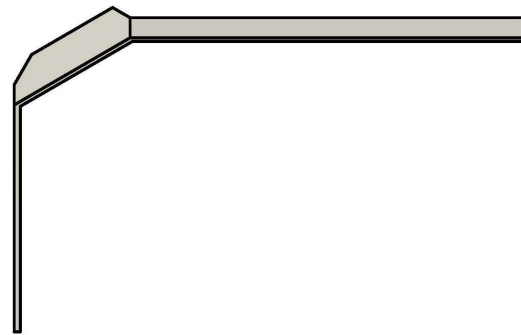


Figure 2.4. Bent wing connector

An experimental procedure to analyze forces in mechanical connections was developed by Pincheira et al. (1998). The connector that was studied consisted of a 6"x1-1/2"x1/4" steel plate with No. 3 bars welded at a 45-degree angle. In this study, a series of ten pilot tests were conducted. The experiment procedure for that research was developed from a series of pilot tests that evaluated a connector for in-plane shear, tension, as well as concurrent shear and tension applied under monotonic and reversed cyclic loading. The experimental procedure developed from the pilot tests observed strength capacities and deformability of the connection and are still used to date. This study set the stage for future research done by Pincheira et al. (2005) where 95 tests were performed on various connector types for in-plane forces. The connectors were embedded in two-inch and four-inch concrete slabs to simulate their embedment in flanges of double-tee girders. The connections in the two-inch slab was a hairpin, stud-welded deformed

bar anchor, bent wing, and an angle welded to the slab's mesh reinforcement. The four-inch slab connections studied was a structural tee, bent wing, bent plate, vector, and angle welded to the slab's mesh reinforcement. The tests performed on the connectors were loaded monotonically and cyclically for in-plane shear, and monotonically for out-of-plane vertical shear. Observations from the experiments confirmed that connectors' in-plane shear strength was affected when concurrent forces were applied. One of the conclusions from Pincheira et al. (2005) stated that "Cyclic in-plane shear loading causes a reduction of shear deformation capacity and ductility in normal mechanical connectors compared to the values expected from monotonic testing."

A similar experimental procedure to Pincheira et al. (1998) was conducted by Shaikh and Feile (2004) on a JVI Vector Connector embedded into 48"x48"x4" concrete slabs. The JVI Vector connector is similar to the bent wing connection shown in Figure 2.4 with the angled wings twisted to be perpendicular to the face of the connection. The reinforcement in the slabs featured diagonal crossed #4 bars with hooks at each corner and wire mesh at mid depth of the slab. A #6 stirrup went around the perimeter of the slab except at the connector. The connectors were comprised of either A36 or stainless-steel. A total of 29 tests were conducted for monotonic and reversed-cyclic horizontal shear with and without tension forces, monotonic tension, and monotonic vertical shear. Two of the tests were embedded into 6-inch thick slabs. The observations from the experiments provided consistent results from similar load categories.

Another study by van de Lindt (2007) evaluated seven types of bent wing mechanical connections. The connectors were approximately the same size with varying embedment angles and were made from two different types of steel which were AISI 304/UNS S-30400 (stainless) and ASTM A-36/ ASME SA-36 (mild). Seven loading protocols were conducted for 70 monotonic and 23 reversed-cyclic tests for horizontal and vertical shear, as well as monotonic

tension. The shear protocols tested the connections in both directions (up/down and left/right) in separate tests. An observation made by van de Lindt (2007) was “In tension, the ductility of the stainless-steel connector was approximately 1.5 to 2 times greater than that of the A-36 mild steel connectors.” Another conclusion made by van de Lindt (2007) stated that “Behavior of the various connectors under monotonic tensile load is approximately the same up to 20kN load.”

Mechanical connections were researched under various load conditions in a two-part set of papers from Naito et al. (2009) and Cao and Naito (2009). Seven connection types were experimentally tested in this research. The first part of the study tested the tension responses and the second part tested the shear responses. Monotonic and cyclic tests were conducted for both responses. The test setup for the research adjoined two slabs with the connections. Some of connections featured a topping poured over them and contained welded-wire rebar. The topped connections were observed to have high initial tensile stiffness. In one of conclusion from the tension responses, Naito et al. (2009) stated “Use of stiff chord and web connections will limit the tensile deformation capacity of the joint and allow the strength of WWR to remain effective.” The shear responses presented in the second part of the research tested the connections with in-plane shear and in-plane shear concurrent with proportional tension. Cao and Naito (2009) stated that “cyclic loading can alter the failure mechanism and often reduce the shear and deformation capacity.” Cao and Naito (2009) said “shear strength of double-tee connections can be conservatively estimated by relying on shear friction or a modified-truss analogy,” in one of their conclusions. Another study by Naito and Ren (2013) discussed evaluation methods for connections where the cyclic procedure for testing is described to have an applied load that captures elastic and inelastic responses when the cycles are applied. The load is incremented in steps after three cycles at the same load. The first increment of cycles is at a small expected

deformation to ensure the data acquisition is accurately performing. The cycles are based upon the respective monotonic test data that anticipated cyclic responses follow the monotonic envelope. This cyclic procedure is typical among experimental studies on mechanical connections.

A numerical analysis of mechanical connectors was researched by Hendricks et al. (2018). The model used an iterative 3-D finite element analysis and a shell model to analyze the flange-to-flange connections. The model was validated with full-scale experimental data on welded connections in a double-tee system from strain gages. The full-scale model was loaded in 300 pound increments up to 1500 pounds. Six load cases were used in the model to estimate deformation of the diaphragm. Each load case applied a 1.5 kip point load at varying locations on the model. Geometric properties and composition of the connection were needed to determine the stiffness of the connection. One of the observations made from the research was that stress distribution varied across connections. The weld stresses in connections require a finite element analysis to be determined and can vary depending on the efficiency of the weld. Double-tee flange compositions need to be taken into consideration when determining connection stresses due to bending of the flange.

The research performed on flange-to-flange precast concrete double-tee mechanical connections have been increasing both experimentally and numerically over the recent decades. There are procedures and models for newly constructed connections, but there is a need to research the rehabilitation and repair of the connections. The current repair method for connections is labor intensive and therefore costly. The repair process requires the pavement topping over connections to be removed so failing welds can be rewelded. Field welded connections can be difficult to get access to because of size restrictions between precast

members. The size restrictions can cause the field welds to be inadequate. Further investigation into repair methods of failing connections is needed to develop the understanding of diaphragm systems throughout their service.

Chapter 3 - Material Properties

Materials used in the experiments were tested for their mechanical properties prior to conducting the experiments to ensure that the materials would provide responses for the desired conditions. The materials that were tested included concrete, which was cast into 4" x 8" cylinders from the batch used to cast the slabs, and the stainless-steel, that was provided by the manufacturer of which the connectors were comprised. The concrete compressive strength tests were performed at Kansas State University and the stainless-steel mechanical properties were provide by the manufacturer. The material properties collected from these tests are provided in Table 3.1 and Table 3.2 for concrete and T316 Stainless-Steel respectively.

Table 3.1. Concrete Properties

Normal-Weight Concrete		
Compressive Strength	4.85	ksi

Table 3.2. Stainless-Steel Properties

T316 Stainless Steel (UNS 31600)		
Yield Strength	51.50	ksi
Ultimate Tensile Strength	91.67	ksi
Elongation	45.47	%
Modulus of Elasticity	29000	ksi

Chapter 4 - Connector Installation

The connectors were embedded into the side edges of the slabs after the slabs finished curing. The installation process was comprised of preparing the connector, cutting slots in the slabs for the connector embedment, mixing of the epoxy resin, and installing and leveling of the connector. Connector preparation required a CNC milling machine, an angle grinder, and acetone. The CNC milling machine was used to mill out the bolt holes for the test fixtures to attach to the connector. Connector faces were lightly ground with the angle grinder to provide a rough surface for the epoxy resin to bond itself to. They were then cleaned with the acetone to remove minor dust and metal shavings. The connectors, shown in Figure 4.1, were ready to be embedded into the slabs which required a slot to be cut into it. The slots were first measured and marked on the center of the edge on the slab with the slot dimensions being a ½ inch wide by 7 inches long by 3-1/2 inches deep, see Figure 4.2. The slots were cut with a 14-inch construction saw held perpendicular to the face of the slab. They were cleaned with compressed air and various brushes to prepare for the epoxy. V-Wrap PF Epoxy Putty Filler was the two-part epoxy resin that was selected and provided by the manufacturer to embed the connectors. The tools required to mix and apply the epoxy were a mixing drill, a putty knife, and a scale. Each part of



Figure 4.1. Typical connectors prepared for embedment



Figure 4.2. Typical slot cut in a slab



Figure 4.3. Final mixing of the epoxy

the epoxy was weighed into separate buckets where one part (Part B) was premixed for two minutes and then added to the contents of the bucket with the other part (Part A). Once the two parts were combined, they were mixed for two more minutes with the mixing drill until a uniform consistency was achieved, see Figure 4.3. The mixed epoxy was transferred to another bucket where it was mixed for two additional minutes. Prior to application and mixing, the slots and connectors were cleaned again and dried completely. The putty knife was used to apply epoxy to the side of the connector that was to be embedded and then thoroughly in the slot to ensure all voids were filled, see Figure 4.4. The connector was inserted into the slot until the connector's top elevation was a $\frac{1}{4}$ inch below the face of the slab and excess epoxy was scraped away with the putty knife. A carpenter's square and level were used during insertion of the connector to maintain perpendicularity with the edge of the slab. Wood blocks were positioned under the connector to hold it in place as the epoxy cured for a week, see Figure 4.5.



Figure 4.4. Application of epoxy putty



Figure 4.5. Connector after installation

Chapter 5 - Experimental Program

The connector's strength capacity was evaluated with three different experimental loading procedures. The three procedures were monotonic tests, cyclic tests, and a flexural test. The monotonic, or static, tests loaded the connectors at a constant rate until failure. Three types of tests were conducted monotonically: axial tension, horizontal shear, and vertical shear. The cyclic tests repeated the horizontal shear and vertical shear tests with incremental steps of displacement that were based upon the monotonic displacement envelopes. Each incremental step had three cycles where the connector was pushed and then returned to zero displacement for each cycle. The flexural test required two slabs adjoined by an embedded connector and then a monotonic load was applied to one slab. The procedures and tests are explained in further detail in their respective sections of this paper.

Multiple connectors were installed in each slab to utilize the slabs more efficiently. The slabs and connectors were numbered to identify which connector was being tested and was denoted as S#C#. The number following the "S" was to identify which slab the connector was embedded into and the number following the "C" was to identify the connector in the lab. For example: S4C10 was the fourth slab connectors were installed into and the tenth connector that was installed. The identification system does not group together connectors by test type, but just by which order they were installed.

The experiments conducted on the connectors used the same equipment in various arrangements and applicable test fixtures for the respective test. The tests were conducted under a load frame that supports a 50-kip hydraulic actuator, which was used to load the connectors. The actuator was pin-connected to the load frame, allowing the actuator to rotate. Therefore, 1-1/2" round steel tubes were fabricated to fix the actuator vertically in place, see Figure 5.1. A 36"

x 60” steel table was used to support the slabs during the tests, see Figure 5.2. The steel table was fixed to the Strong Floor in the laboratory using tie-down anchors that go through an HSS8x6x3/8 steel tube that was filled with concrete, see Figure 5.3. Each test type required fabrication of additional supports to restrict unwanted movement of the slab, such as columns, brackets, anchor bolts, steel beams, and anchor bars, which are described in detail in their respective test procedure section.



Figure 5.1. Actuator fixturing



Figure 5.2. Steel table



Figure 5.3. Steel tube filled with concrete

The connectors were loaded from the actuator by test fixtures with bolted connections that were provided by Structural Technologies Inc. The provided test fixtures included a 1-1/2” threaded actuator adapter, 5/8”x1-1/2” bars, a 3-inch long 5x5x3/8 angle, 5”x4-1/2”x3/8” plates, 3/4” bolts, and 4”x3”x1/8” washer plates, see Figure 5.4. The actuator adapter screwed into the actuator’s load cell and had two vertically aligned bolt holes creating a fixed connection. The

loading bars varied in length and were used to transfer the load from the actuator adapter to the connector. The angle and plates were used to attach the loading bars to the connectors for the horizontal and vertical shear tests, respectively. The washer plates were used as spacers to fill the gaps and to limit lateral (out-of-plane) bending stresses in the test fixture. The test fixtures were assembled together using the ¾” bolts. Throughout the course of testing there were some modifications to the test fixtures.

The test fixtures alterations were made after observing their performance on the first tensile and horizontal shear tests. The tensile test fixture was remade with two longer loading bars that attached the actuator adapter and the connector directly. This alteration made the distance from the actuator to the connector shorter with fewer bolted connections. The horizontal shear test fixture required the most alterations from the original single loading bar to angle fixture because the loading bar began to bend in the same plane as the slab faces when force was applied. The initial solution was to add a brace to the loading bar, but the test setup did not allow for a brace with enough support to be added. The fixture was instead built-up with three loading bars. The steel angle, that was attached to the connector, had plates welded on both sides of it to increase stiffness. Since the other two test fixtures needed to be altered after their first tests, the vertical shear fixture was altered before testing by reducing the distance from the actuator to the connector to reduce effects of buckling of the loading bar.

The tests were conducted using displacement-control of the hydraulic actuator. This was used instead of force-control to prevent sudden failure of the specimen from trying to pick up higher load demand while the slab was degrading due to concrete cracking. The data that was recorded from the tests included actuator force, actuator displacement, string potentiometer displacement, and time. All data was acquired by an MTS data acquisition system and a sample

output screen is shown in Figure 5.5. After each test was concluded, the recorded data was imported into Excel files to process the data. The results are discussed later in this report. The string potentiometer was attached to the test fixtures to capture the connector displacement in-line with the actuator load for each test and is shown in their respective procedure sections.

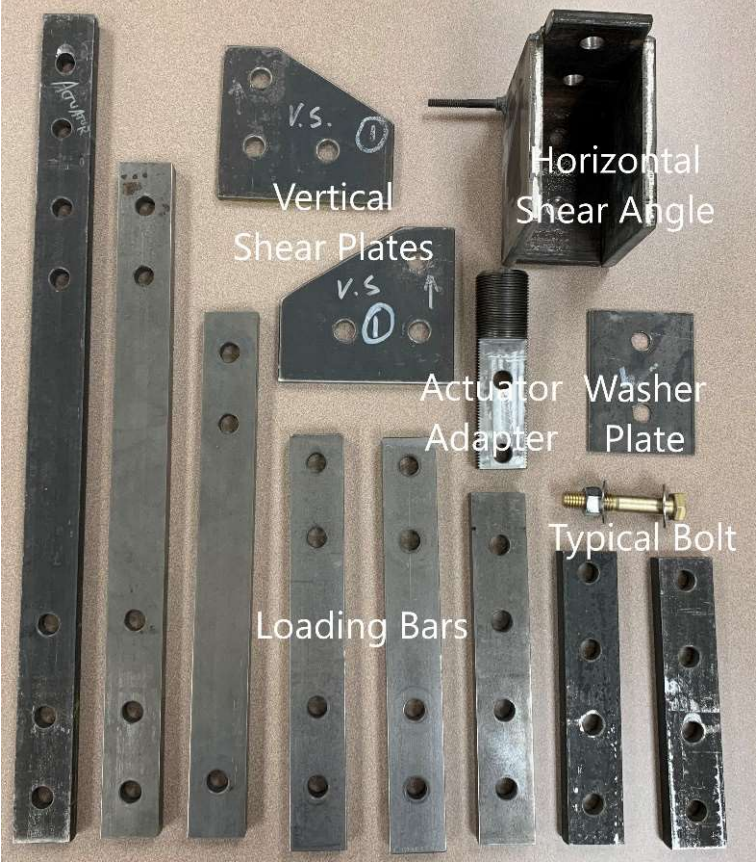


Figure 5.4. Test fixture components

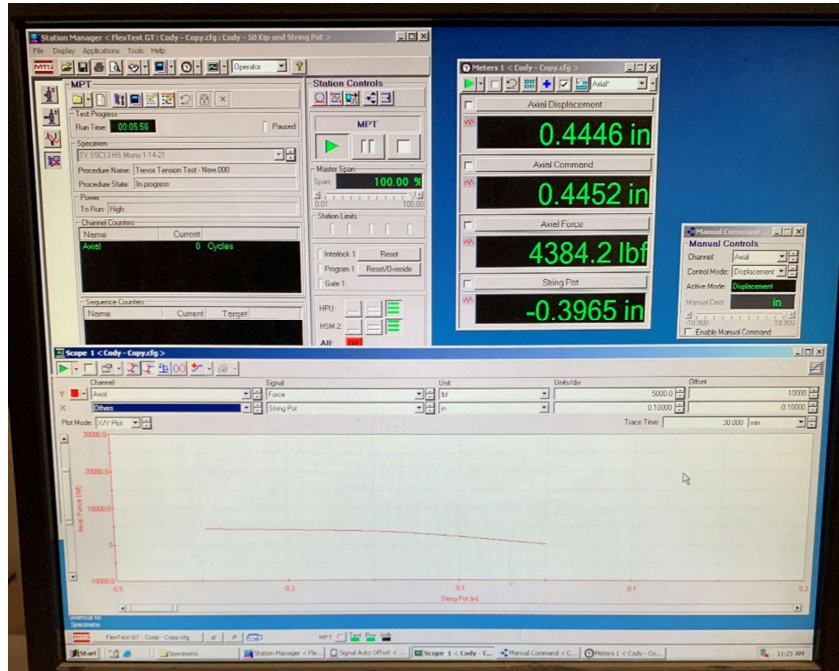


Figure 5.5. MTS data acquisition system sample output screen

Monotonic Loading

Axial Tension Test

The axial tension tests required the loading to be applied perpendicular to slab's edge to create a pure tension force in the connector. The test setup needed the concrete slab to be oriented vertically on the bottom edge of the slab (the edge opposite from the connector to be tested) so that the connector was directed upwards in line with the actuator. The steel table was positioned under the load frame with the long side of the table parallel to the face of the slab, see Figure 5.6. A W5x16 steel beam was secured to the feet of the table using clamps so the bottom slab edge was fixed in place during testing. The edge of the slab with the connector embedded in it was fixed on the corners with two 1-1/2" round steel columns that spanned vertically up to the load frame, see Figure 5.7.

The test fixture for tensile loading was composed of the actuator adapter, two loading bars and steel washer plates. The configuration of the test fixture included the loading bars to be

attached to both sides of the actuator adaptor and the embedded connector with a total of four bolts, two in the adapter and two in the connector, see Figure 5.8. Steel washer plates were used to fill the gaps between the connector and loading bars. The string potentiometer was attached to the nearest bolt to the connector on the test fixture, see Figure 5.9. The actuator operated at a displacement-controlled rate of 0.0125 inches/minute upward.

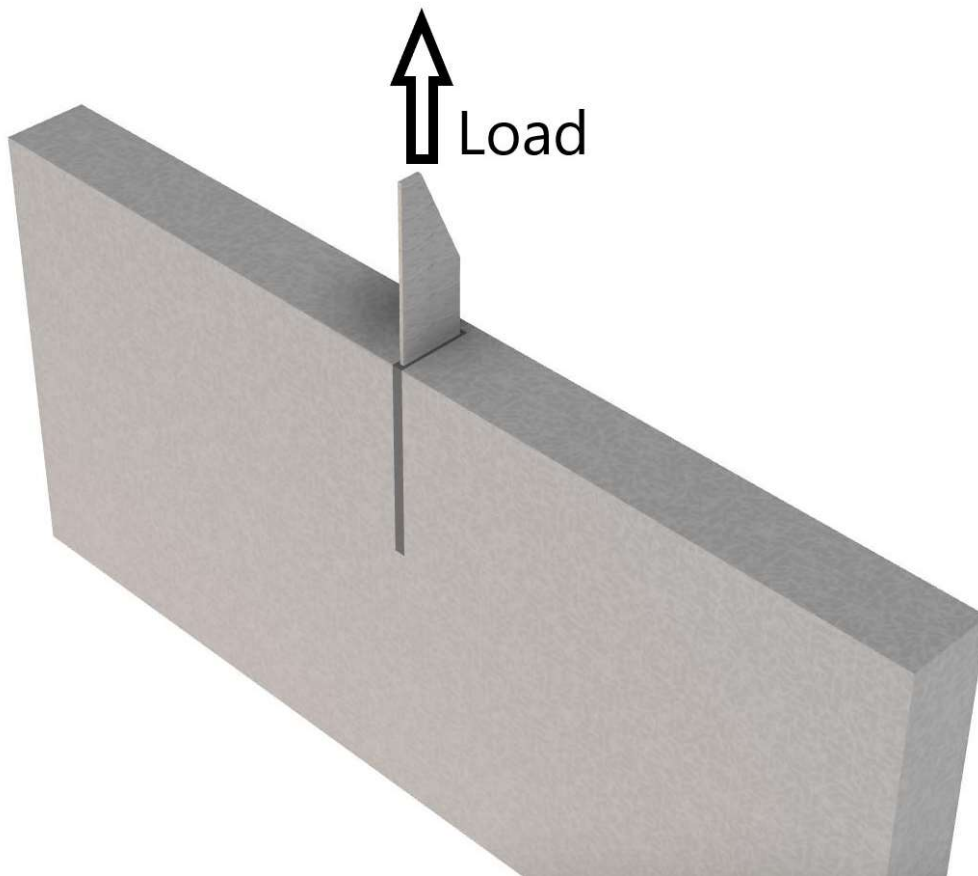


Figure 5.6. Axial tension applied load direction

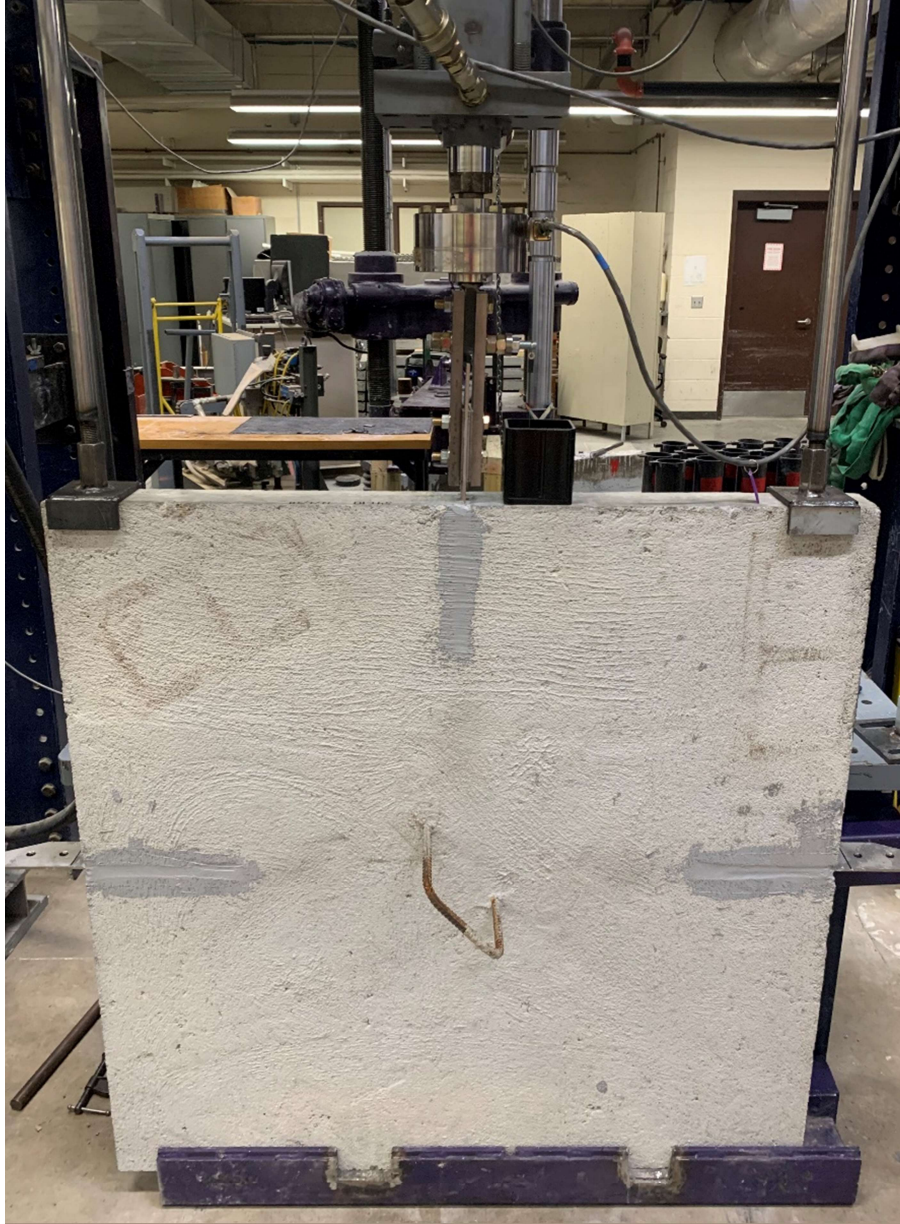


Figure 5.7. Axial tension test fixities



Figure 5.8. Axial tension test fixture



Figure 5.9. Axial tension string potentiometer placement

Monotonic Horizontal Shear Test

The horizontal shear tests required the connector to be loaded in the direction parallel to the plane of the slab to generate a horizontal force on the connector. The test setup needed the slab to be oriented vertically on the bottom edge of the slab (the edge adjacent to the connector to be tested) with the connector's face being perpendicular to the actuator, see Figure 5.11. The steel table was positioned outside of the load frame and on one side of the actuator to align the slab in the same vertical plane as the actuator with the long side of the table parallel to the face of the slab, see Figure 5.10. The W5x16 steel beam used to support the slab in the tensile tests was used similarly for fixing the bottom edge of slab in these tests as well. The top edge of the slab was secured using one 1-1/2" round steel column to fix the corner of the slab near the connector.

Two mounting brackets were bolted to the table and anchored to the slab to secure the other top corner of the slab, see Figure 5.12. The horizontal shear tests required the loading to be applied to the connector on the side edge of the slab which will create an overturning moment of the slab. To resist the overturning moment, a 1-1/8" hole was drilled through the slab in the bottom corner opposite of the loaded connector to insert a 1-inch through rod that was tied down to the Strong Floor, see Figure 5.12.

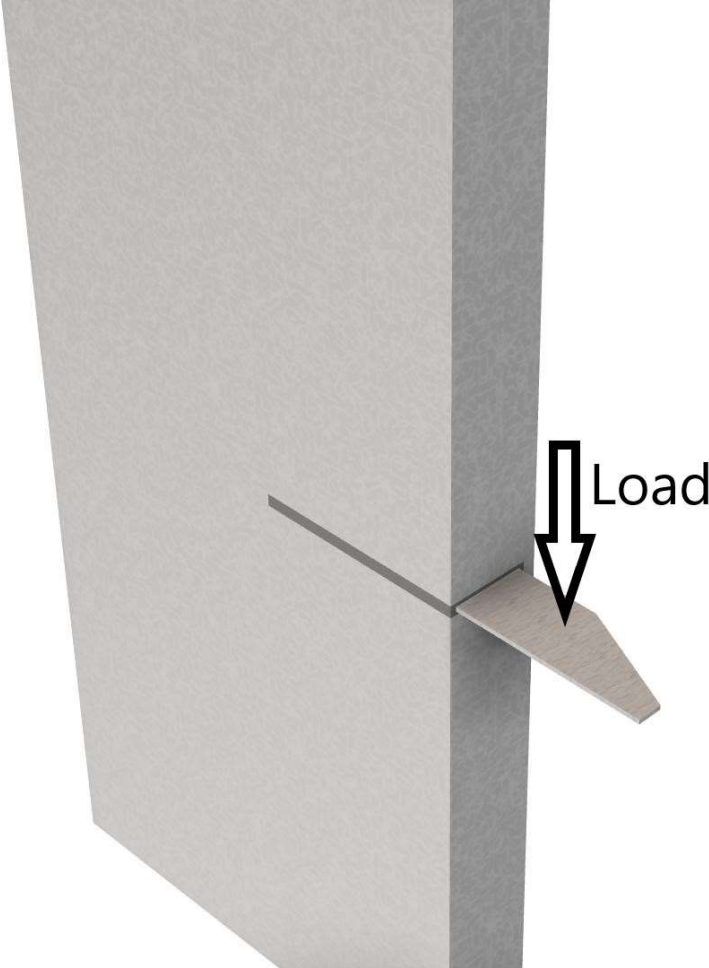


Figure 5.10: Horizontal shear applied load direction



Figure 5.11. Horizontal shear table and slab orientation



Figure 5.12. Horizontal shear slab fixturing

The test fixture used for the horizontal shear tests was composed of the actuator adapter, five loading bars, and a built-up angle. The test fixture configuration was two shorter loading bars that were bolted on both sides of the actuator adapter. The other end of the two loading bars was bolted to a longer loading bar that spans from the tip of the actuator adapter down to the connector, see Figure 5.13. The longer loading bar has two more loading bars on either side and was bolted to the built-up angle which was bolted to the connector's face. The test fixture used a total of ten bolts. The string potentiometer was attached to a rod that was welded onto the built-up angle in-line with the actuator, see Figure 5.14. The actuator operated at a displacement-controlled rate of 0.075 inches/minute downward.



Figure 5.13. Horizontal shear test fixture



Figure 5.14. Horizontal shear string potentiometer placement

Monotonic Vertical Shear Test

The vertical shear tests required the connector to be loaded in the direction perpendicular to the plane of the slab to generate a vertical shear force on the connector. The test setup needed the slab to be oriented horizontally on the bottom face of the slab with the connector's face being parallel and in line with the actuator, see Figure 5.15. The steel table was centered and positioned outside of the load frame with long edge of the table parallel to the edge of the slab with the embedded connector to be tested. The slab was centered on the table with the connector embedded slab edge flush with the edge of the table, see Figure 5.18. The table was leveled and secured to the Strong Floor using tie downs through the concrete filled HSS beam underneath the

table top, see Figure 5.17. The slab was fixed to the table with a steel channel and all-thread rods, see Figure 5.17.

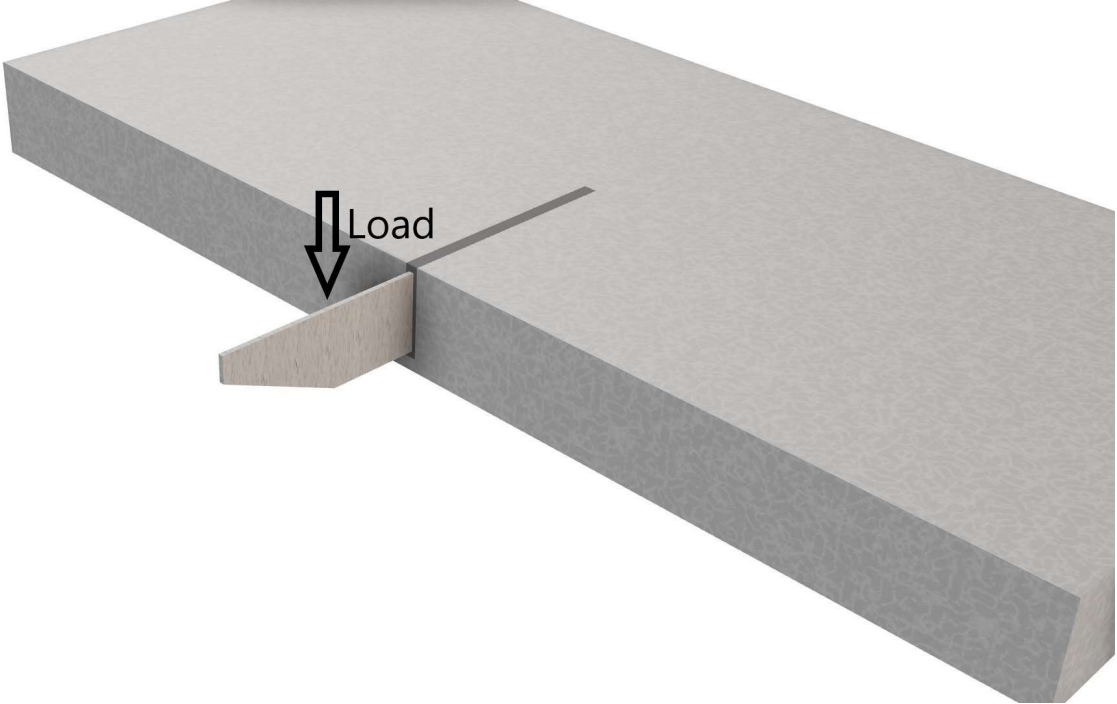


Figure 5.15. Vertical shear applied load



Figure 5.16. Vertical shear slab orientation



Figure 5.17. Vertical shear table and slab
fixturing

The test fixture used for the vertical shear tests was composed of the actuator adapter, five loading bars, steel washer plates, and the 3/8" plates. The configuration of the test fixture was two loading bars bolted on both sides of the actuator adapter with the other end of the two loading bars bolted on either side of a third loading bar. The third loading bar was bolted between two lower loading bars that span to the connector, see Figure 5.19. The 3/8" steel plates were bolted to the other end of the lower loading bars and on each side of the connector's faces, see Figure 5.20. A total of nine bolts were used to assemble the test fixture. The string potentiometer was attached to the bolt that went through the connector and in line with the actuator centerline, see Figure 5.18. The actuator was operated at a displacement-controlled rate of 0.025 inches/minute downward.



Figure 5.18. Vertical shear slab alignment and string potentiometer placement



Figure 5.19. Vertical shear test fixture



Figure 5.20. Vertical shear test fixture (side view)

Cyclic Loading

The experimental program for the cyclic loading was determined from the estimated yield displacement of the monotonic tests for horizontal shear and vertical shear. The goal of these tests was to determine the effect of repeated pushing on the connector and to obtain a load-displacement response within the respective test's monotonic load-displacement envelope. A reverse-cyclic loading was not followed to mimic the actual cyclic nature of the loading in terms of vehicle loading and unloading. The cyclic test protocol incremented steps of displacement with three cycles per step with the duration for each cycle being 10 seconds. The actuator pushed downward for five seconds and then pulled back to zero displacement for the next five seconds of each cycle. The first step in the protocol displaced the actuator 0.010 inches to ensure the instrumentation was working properly. The subsequential steps for each of the test protocols are presented in detail in the following sections.

Cyclic Horizontal Shear Test

The cyclic horizontal shear test setup followed the same displacement envelope that was used in the monotonic horizontal shear tests, so comparable responses could be examined, refer to Figure 5.21. The estimated yield displacement from the monotonic tests was approximately 0.125 inches. Displacement increments of 0.025 inches/step were used until the actuator displacement reached 0.250 inches, then the increments increased to 0.100 inches/step until 0.750 inches/step, see Figure 5.21. The smaller increments at the beginning of the test was intended to capture when the connector became permanently deformed.

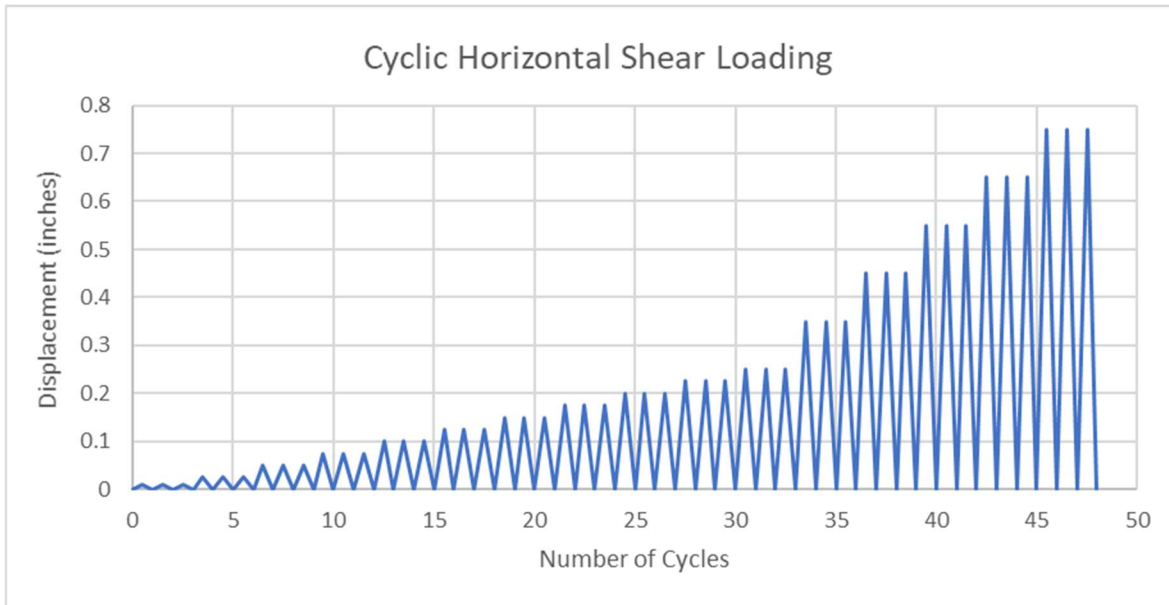


Figure 5.21. Cyclic horizontal shear loading

Cyclic Vertical Shear Test

The cyclic vertical shear test setup followed the same displacement envelop as the monotonic vertical shear test except for the addition of a longer loading bar in the test fixture, see Figure 5.23 and Figure 5.24. The longer loading bar allowed another bolt to be added to the fixture, increasing rigidity. The monotonic vertical shear tests experienced peak load at an average deformation of approximately 0.550 inches. Displacement increments of 0.050 inches/step were used until the specimen failed or one inch of displacement was achieved, see Figure 5.22.

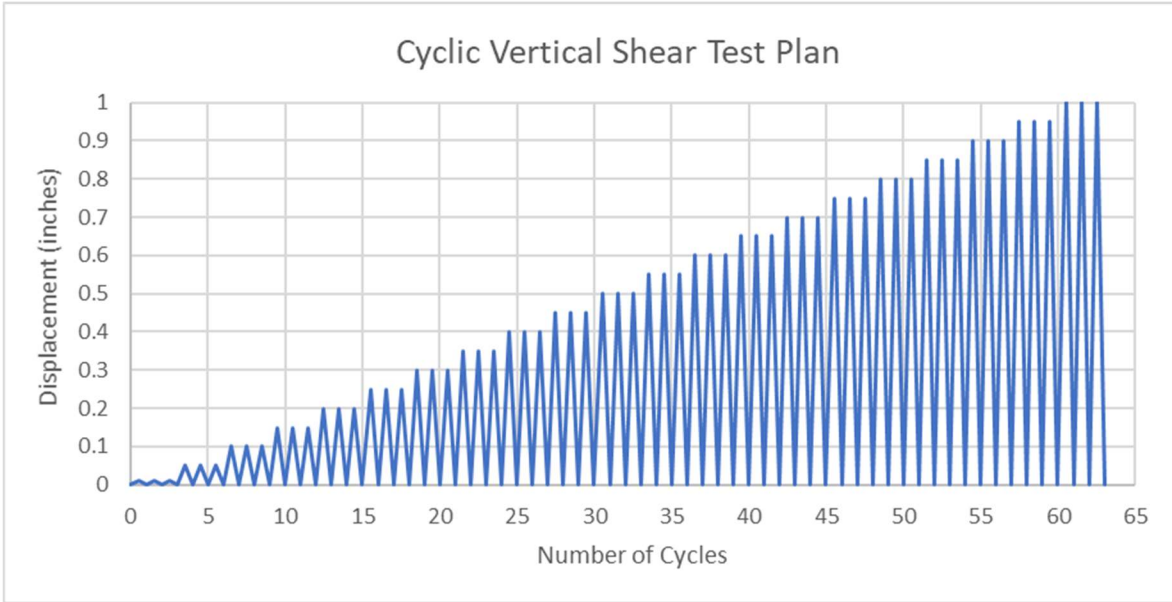


Figure 5.22. Cyclic vertical shear loading



Figure 5.23. Cyclic vertical shear test fixture



Figure 5.24. Cyclic vertical shear test fixture

Flexural Test

The flexural test was designed to analyze the response of the connector when it was embedded into two cantilevered slabs that would replicate the connection between flanges of two precast double-tee concrete beams, see Figure 5.25. The two slabs that were used for this test were S8 and S9. Two sides of S8 were used for cyclic horizontal shear tests and S9 was not used in a prior test. The previous tests performed on S8 would not impact the results on this test because the slab did not experience concrete cracking and the embedments were not in the cantilevered span.

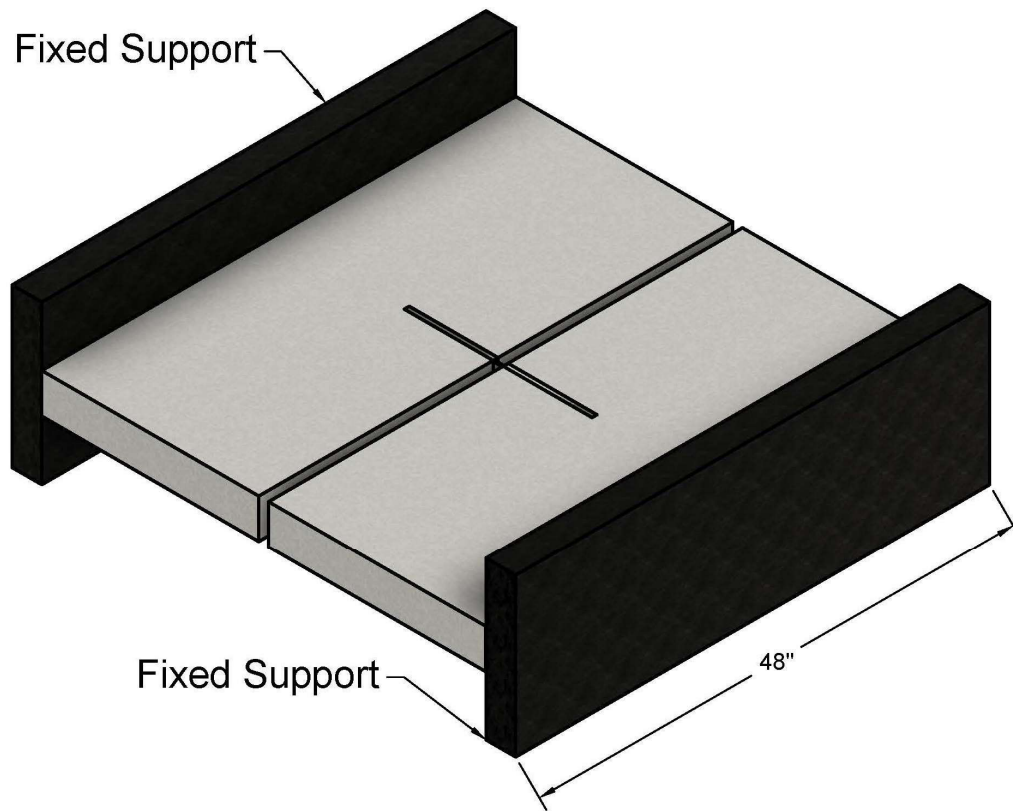


Figure 5.25. Flexural test setup

The test setup for the flexural test required two steel loading tables that were used to fix the slabs. A grid was marked on the floor of the lab under the actuator with chalk lines to align the tables. The tables were oriented with longer edge being parallel to the direction of the

connector's embedment in the slabs. The short edges of the tables were positioned 45 inches apart from each other so the slabs would be cantilevered 22 inches on each table with a one-inch gap of separation between the slabs. The clear gap was centered directly under the actuator and each table's center line in the same plane as the connector. The end of the tables opposite from the cantilevered slabs were tied down to the Strong Floor of the lab using concrete filled HSS steel tubes to prevent the tables from overturning. The slabs were prepared after the tables were positioned and secured.

The connector and slab preparation for this test followed the same process as previously detailed in Chapter 4 - Connector Installation. The faces of the connector used in this test were lightly ground on both sides and cleaned with acetone, see Figure 5.26. Alignment lines were drawn on the connector seven inches in from the tips to ensure an equivalent embedment length of the connector in both slabs with an exposed gap of one inch. The slabs were prepared separately outdoors from the lab before the test. The slots for the connector were cut into the center of the edge of the slabs. The slabs were brought inside to the lab where the slots were cleaned thoroughly with compressed air and acetone. A line was drawn with a marker 22 inches from the edge of the slab in which the slots were cut to identify the cantilevered span, see Figure 5.27.



Figure 5.26. Flexural test connector prepared for installation



Figure 5.27. Flexural test cantilevered slab

A forklift was used to lift the slabs onto the loading tables and the slabs were positioned on the tables with an overhead crane. The slabs were cantilevered and centered on the tables which aligned the slots under the actuator with the one-inch gap of separation, see Figure 5.28. A ratchet strap and steel plates were used to temporarily secure the slabs on the tables while holes were drilled through the slabs for the main fixtures. Each slab was fixed with three 3x3x3/8 angle sections and a 6-inch steel channel. The angles and channel were bolted to the steel table with all-thread rods that went through the eight holes that were drilled in each slab, see Figure 5.29. The ratchet strap and steel plates were removed when the slabs were secured with the steel angles and channel. The edges of the slab adjacent to the edge that the connector would be embedded extended 6 inches past the edge of the table due to the limited table size, see Figure 5.30. The connector was installed after the slabs were fixed to the tables.



Figure 5.28. Aligned slots for the flexural test



Figure 5.29. Slabs fixed to the tables for the flexural test



Figure 5.30. Slab overhang on the tables

The epoxy putty was mixed to the manufacturer's specifications, which was discussed previously. Epoxy was applied with a putty knife in the slots and on the faces of the connector, except in the area between the alignment lines, see Figure 5.31. The connector was inserted into the slots until the top of the connector was below the top face of the slab, shown in Figure 5.32 and the alignment lines were flush with the edges of the slabs. Excess epoxy was scraped away and the top surface was smoothed out, see Figure 5.33. The epoxy cured for seven days and then the test fixture was installed.



Figure 5.31. Connector installation for the flexural test



Figure 5.32. Connector inserted below the top face of the slabs



Figure 5.33. Installed connector for the flexural test

The test fixture for the flexural test was designed to apply the load on only one of the slabs on top of the connector's embedment. A spreader beam with two roller supports was used to offset the load applied from the actuator, which was located above the connector, see Figure 5.34. The spreader bar was a built-up shallow I-beam section with web stiffeners and the rollers were two inches in diameter that were in between four-inch plates. The plates had a rounded indentation that matched the outer diameter of the rollers so rotation could occur, but translation could not. The placement of the rollers allowed the load to be transferred to the steel table under S8 and to the cantilevered slabs. The roller support that applied the load to the slabs was placed 3-1/2 inches from the connected edge of S9, or at the middle of the embedment of the connector, see Figure 5.36. The other roller support was placed in between the slab-to-table fixtures on the S8 directly above the table, see Figure 5.37. An additional 1/2-inch plate was added above the rollers that provided extra clearance of the slab-to-table fixture. A ratio of the lengths was used

to determine the load applied on the connector from the actuator and is written in Equation 5.1. The rollers were located 44 inches apart and the actuator was located over the center of the one-inch gap. A third roller that represented the actuator was placed on top of the spreader bar to verify the measurements, but was removed before the test started. The length ratio for the roller that applied the load was 40 divided by 44 or 90.9% of the actuator load. This length ratio was input into the raw data of the Excel file generated from the data acquisition system. The data acquired for this test was actuator force, actuator displacement, and string potentiometer displacement. The string potentiometer was attached to a rod clamped to the slab located in the same plane as the roller support that applied the load to track the actual displacement of the test, see Figure 5.38. Actuator displacement was not the real displacement of the test because the actuator did not apply the load directly to the slabs. The load was applied to the spreader bar with a four-point bending test fixture that was attached to the actuator shown in Figure 5.39. After the test fixture was installed, the spreader bar was observed to have been installed about a half inch off of center. The eccentricity of the load on the spreader bar was assumed to be negligible due to the stiffeners in the spreader bar having adequate load transfer ability. The actuator operated at a monotonic displacement-controlled rate of 0.100 inches/minute downward.

Equation 5.1: Load applied to the connector

$$P_{connector} = \frac{L_{S8, Roller}}{L} \times P_{actuator}$$

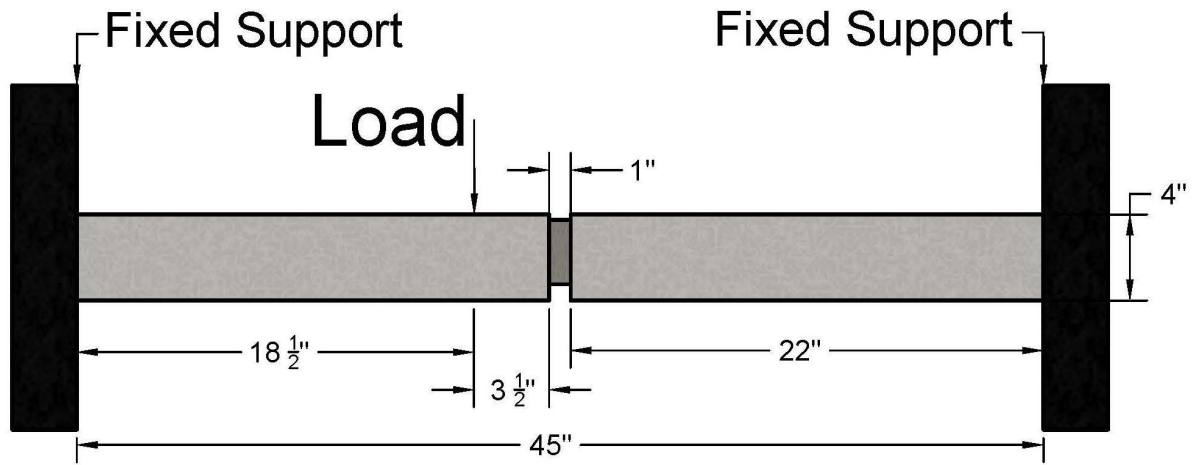


Figure 5.34. Flexural test applied load location



Figure 5.35. Flexural test fixture



Figure 5.36. Roller over the embedded connector



Figure 5.37. Roller located over the steel table



Figure 5.38. Flexural test string potentiometer placement



Figure 5.39. Actuator test fixture

Chapter 6 - Results and Discussions

The results from the conducted experiments provided data that was used to generate a force verses displacement relationship for both the actuator displacement and the string potentiometer displacement. The MTS data acquisition system recorded several data points per second. The results were narrowed down using a data sorting macro in Excel to capture the general shape of the total plots and large changes in load and displacement. Displacement-controlled testing produced cracks in the concrete gradually as the connector was being loaded by the applied deformation. This allowed for the cracks to be tracked as they appeared during the test. The cracks were traced with a black marker to ensure that the cracks did not disappear due to the cracks closing when the specimen was unloaded, and to make them more visible in pictures.

The string potentiometer was used as an additional displacement measurement to track the actual displacement of the connector and not the actuator displacement. After interpretation of the data, the string potentiometer displacement data was considered to be the most accurate displacement data. The actuator displacement does not account for the bolt hole tolerances and deformation caused from the test fixtures being loaded repeatedly, which caused the bolt holes to elongate. This was why the string potentiometer data is less than that of the actuator displacement in all the tests included in the following results. The results from the individual tests are elaborated in their respective test results sections.

Monotonic Loading

Axial Tension Test

Axial tension tests were the first tests conducted in this research. The connectors that were tested were S1C1, S2C4, S3C7, and S4C10. The tensile force-displacement plots generated from the data show a linear relationship until failure, which was at the maximum load. The average maximum load for the tests was 13,220 lbf, the average actuator displacement at the maximum load was 0.1400 inches, and the average of the recorded string potentiometer displacements at the maximum load was 0.0713 inches. The maximum force and displacements for each test is displayed in Table 6.1. The test plots for the four tension tests were presented in terms of the axial tension force versus the actuator displacement and the string potentiometer displacement and are shown in Figure 6.1 and Figure 6.2, respectively.

Table 6.1. Axial tension test results

Connector	Force (lbf)	Actuator Displacement (inches)	String Potentiometer Displacement (inches)
S1C1	13425	0.173	-
S2C4	13548	0.150	0.042
S3C7	13681	0.115	0.096
S4C10	12227	0.122	0.076
Averages	13220	0.140	0.071

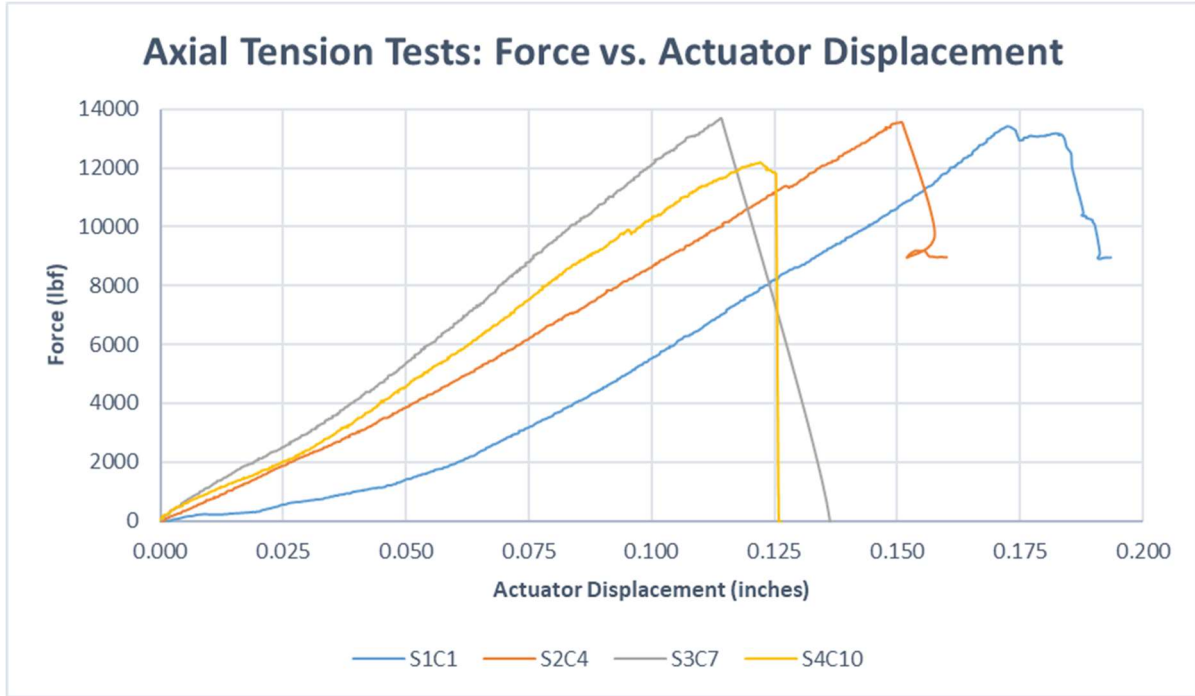


Figure 6.1. Axial tension tests force versus actuator displacement plot

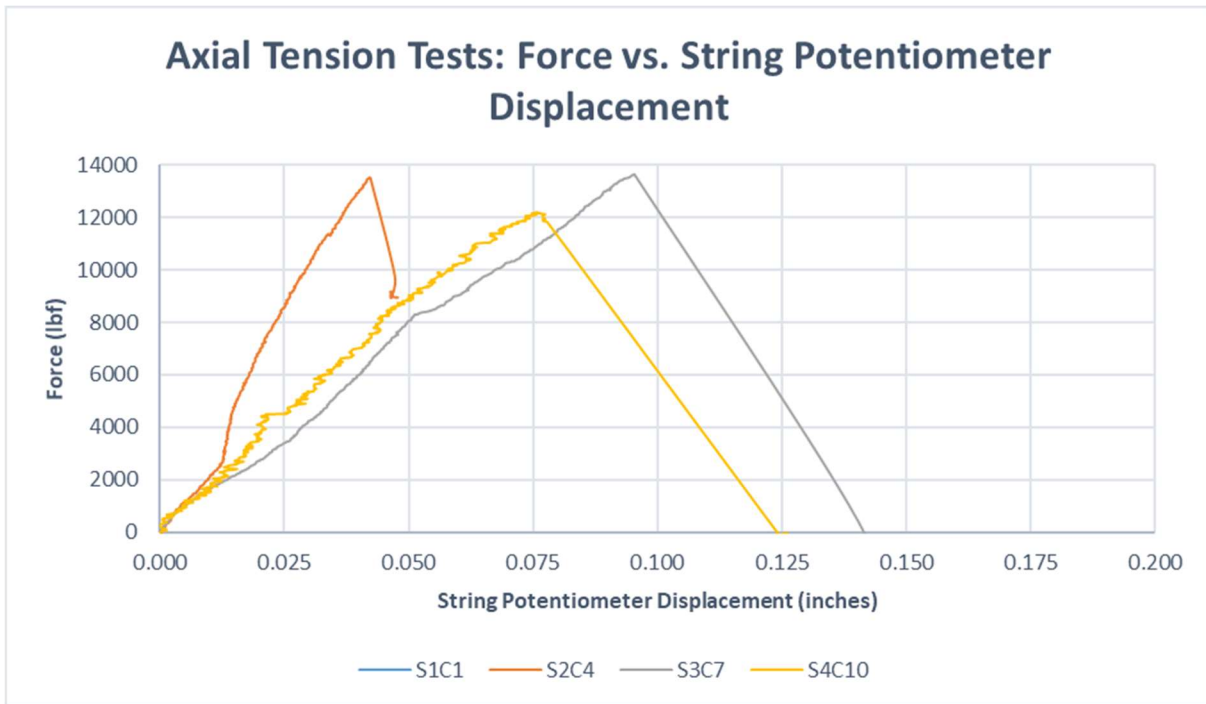


Figure 6.2. Axial tension tests force versus string potentiometer displacement plot

The first axial tension test was on the connector named S1C1. The string potentiometer displacement data was not recorded during this test due to an MTS data acquisition system program error. The actuator displacement recorded for this test was not accurate due to the insufficient supports to restrain the slab from movement during the test. After this test, the steel columns were fabricated and added to the test setup to hold the slab from slightly lifting up during the application of axial tension, as mentioned in the experimental program chapter. This was uniformly done for the other three tensile tests. The force achieved during this test was in the same range as the other tensile tests and was assumed to be accurate. This assumption was verified by the failure mode of concrete cracking under axial tension in a diagonal pattern, which was the same as in tests for S2C4 and S4C10. The cracking of S1C1 is shown in Figure 6.3 and Figure 6.4.



Figure 6.3. S1C1 top slab face cracking



Figure 6.4. S1C1 bottom slab face cracking

The second axial tension test was on the connector named S2C4. During this test the string potentiometer experienced an inconsistent supply of voltage causing the data output to not be accurately measured after a tension force of about 2200 lbf. The entire string potentiometer system was rebuilt, and no further problems were experienced with string potentiometer data

during the two remaining tests. The slab was sufficiently fixed in place and achieved the second largest load of the tensile tests. Figure 6.5 and Figure 6.6 show the cracking around S2C4 after testing.



Figure 6.5. S2C4 top slab face cracking



Figure 6.6. S2C4 bottom slab face cracking

The third axial tension test was on the connector named S3C7. This test achieved the highest loading of the tensile tests. The failure mode of this test was from the connector instantaneously debonding and sliding outwards away from the epoxy, which caused all the strength to be lost. The failure mode is shown in Figure 6.7. When the epoxy bond failed, it

caused a significant increase in displacement by 0.047 inches on the string potentiometer data and by 0.022 inches in the actuator displacement data. Debonding of the connector from the epoxy only occurred during this test. This was the only test that the concrete slab did not crack in, as seen in Figure 6.8. However, it was noted that this slab was outside the night before the test and had some ice frozen on the connector. All the ice was removed from the connector and slab when it was brought into the laboratory and was indoors for about an hour before testing. This exposure to cold weather was believed to have affected the epoxy resin making it the weak link in this test. Interestingly enough, the ultimate load of this test was still found to be similar to those of the other three tests that failed by concrete cracking.



Figure 6.7. S3C7 after the epoxy slipping from around the connector



Figure 6.8. S3C7 No visible cracking after testing

The fourth axial tension test was on the connector named S4C10. When comparing the force versus displacement plots of this test, it was observed that at the maximum load, the displacement of the string potentiometer was half that of the actuator displacement, however after failure the string potentiometer displacement almost matched the actuator displacement. This test was the second test that the connector embedment lost all its strength at failure. Figure 6.9 shows the failure of this test from concrete cracking in tension. It is worth mentioning that the response of this connector was close to that of specimen S3C7, seen in Figure 6.1.

Concrete cracking in tension was the most common failure mode of the axial tension tests, occurring in three out of the four tests. This result was anticipated due to the connector's high tensile strength properties. All four tests failed instantaneously as load significantly dropped and displacement jumped. When the concrete cracked in tension, the cracks appeared around the

connector's embedment in the slab and typically formed along the planes where the epoxy was bonded with the slot cut into the slab. From the results of the S3C7 test, the bond between the connector and epoxy should be further investigated to see if the load achieved during that test was the maximum tension strength of the epoxy.



Figure 6.9. S4C10 concrete cracking in tension

Monotonic Horizontal Shear Test

The monotonic horizontal shear tests were the second type of test that was conducted and was tested on four connectors named S2C6, S1C2, S1C3, and S5C13. The force versus displacement plots generated from these tests produced a bi-linear curve, shown in Figure 6.10 and Figure 6.11. The plots can be divided into three regions: the linear-elastic region, the strain hardening region, and ultimate yield region and are provided in Table 6.2,

Table 6.3, and Table 6.4. The linear-elastic region occurred at the beginning of the tests until a load of about 2,575 lbf was achieved and the connector began to permanently deform. Once permanent deformation began, the connector entered the strain hardening region at a load of 3,710 lbf and was elongated without gaining a noticeable load increase until about 6,827 lbf

was applied. After the connector went through strain hardening, the load increased very rapidly over small displacements relative to the strain hardening region. Testing was stopped when the applied load surpassed 20,000 lbf due to the test fixture bending and not because the embedment of the connectors failed.

Table 6.2. Horizontal shear linear-elastic region

Linear-Elastic Region			
Connector	Force (lbf)	Actuator Displacement (inches)	String Potentiometer Displacement (inches)
S2C6	2020	0.059	0.039
S1C2	2418	0.155	0.095
S1C3	2941	0.125	0.109
S5C13	2922	0.174	0.147
Averages	2575	0.128	0.097

Table 6.3. Horizontal shear at the start of strain hardening region

Start of Strain Hardening Region			
Connector	Force (lbf)	Actuator Displacement (inches)	String Potentiometer Displacement (inches)
S2C6	4066	0.431	0.273
S1C2	3425	0.368	0.262
S1C3	3483	0.197	0.174
S5C13	3868	0.290	0.251
Averages	3710	0.322	0.240

Table 6.4. Horizontal shear at the beginning of ultimate yield region

Beginning of Ultimate Yield Region			
Connector	Force (lbf)	Actuator Displacement (inches)	String Potentiometer Displacement (inches)
S2C6	7087	1.079	0.845
S1C2	6341	1.260	1.051
S1C3	7293	1.026	0.954
S5C13	6588	1.017	0.927
Averages	6827	1.096	0.944

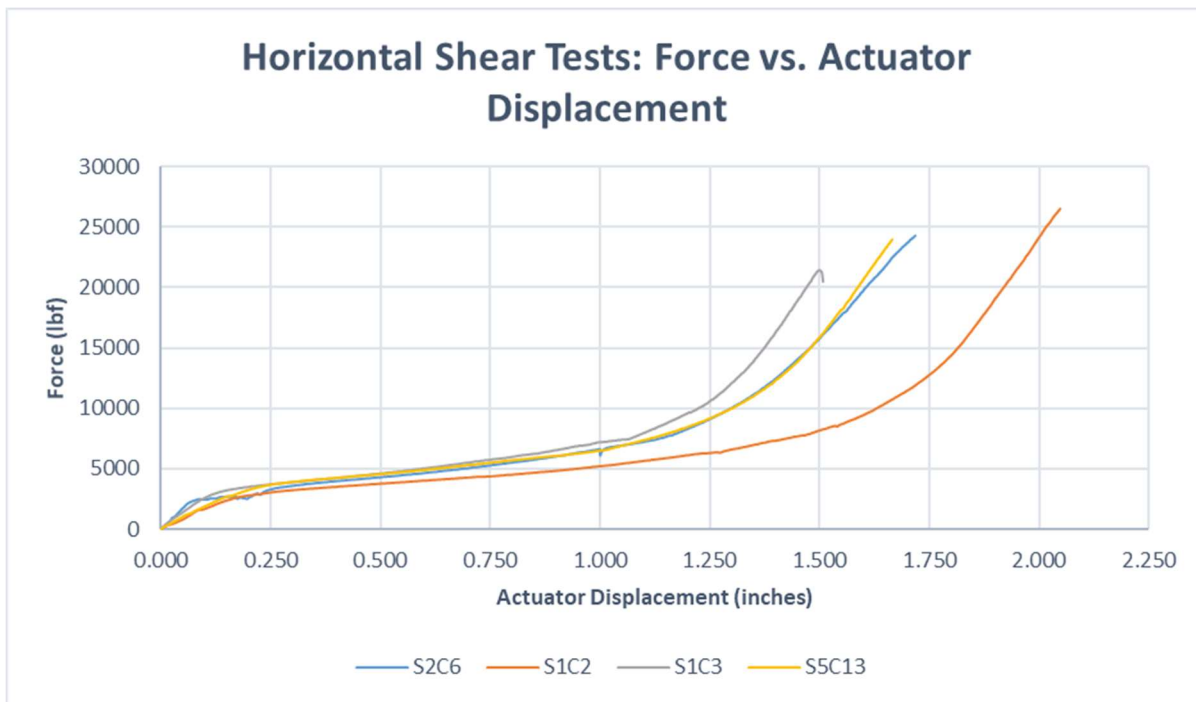


Figure 6.10. Horizontal shear tests force versus actuator displacement plot

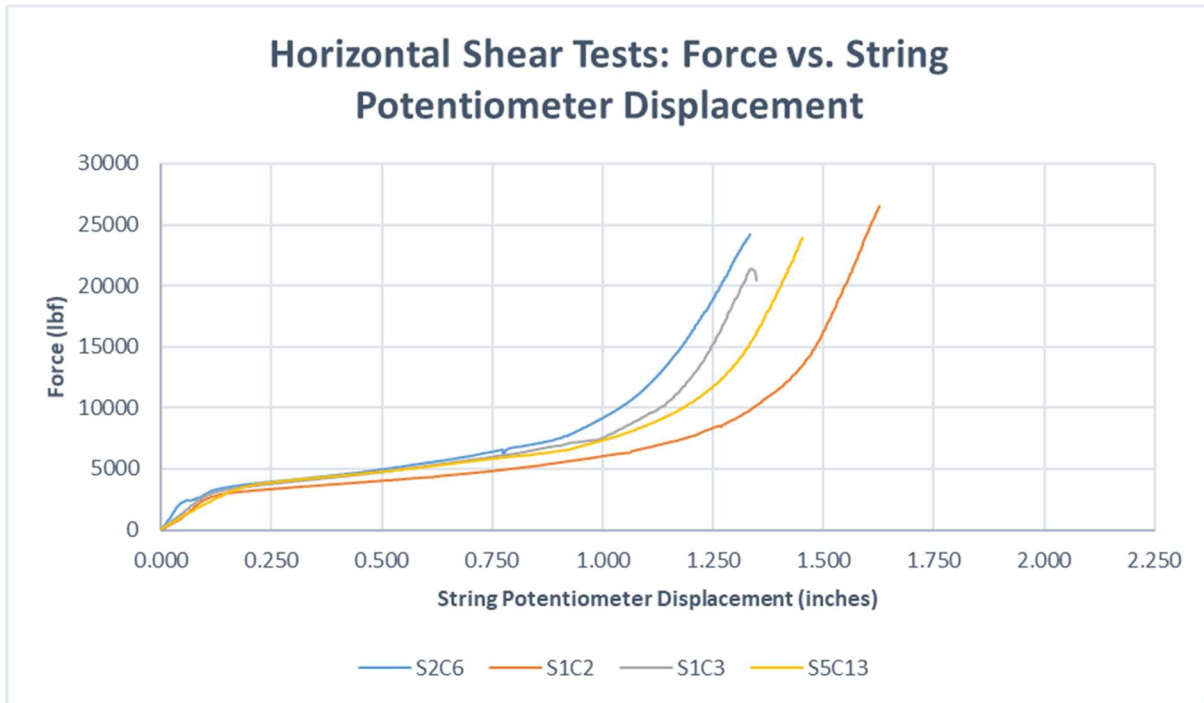


Figure 6.11. Horizontal shear tests force versus string potentiometer displacement plot

The horizontal shear test results for the four tests provided consistent data for every test. The only test that provided a failure mode was on S1C3 when the slab cracked away from the connector's embedment, shown in Figure 6.12, and the other three tests (S1C2, S2C6, and S5C13) were stopped after the load was greater than 20,000 lbf to prevent permanent damage to the test fixture caused by buckling. All the connectors separated from the epoxy around 3,000 lbf, shown in Figure 6.13. It was assumed that the connector had been permanently deformed after 3,500 lbf of applied load, see Figure 6.14. The connectors had noticeably rotated at the embedment at 6,000 lbf, shown in Figure 6.15. At around 10,000 lbf, the concrete under the connector started to crush and spall on either side of the connector, shown in Figure 6.16.



Figure 6.12. S1C3 cracking away from the connector



Figure 6.13. Typical connector-epoxy separation

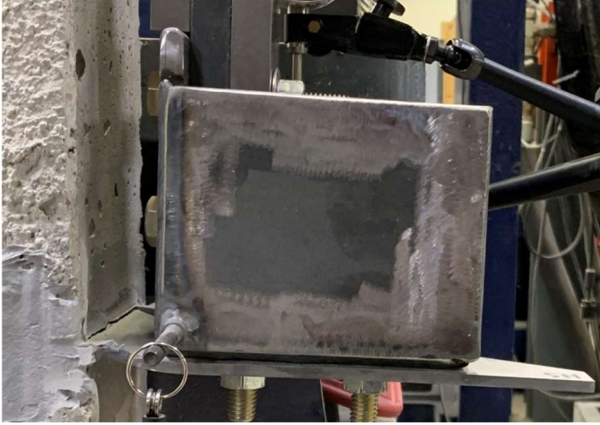


Figure 6.14. Typical start of permanent deformation of the connector



Figure 6.15. Typical connector rotation around 6,000 lbf



Figure 6.16. Typical crushing of concrete under the connector

Monotonic Vertical Shear Test

The monotonic vertical shear tests were the third type of test that was conducted and was tested on four connectors named S6C15, S6C16, S7C17, and S7C18. The force versus displacement plots generated from these tests produced curves with multiple drops in load throughout the duration of the tests and is shown in Figure 6.17 and Figure 6.18. The ultimate load and displacements for each test is provided in Table 6.5.

Table 6.5. Vertical shear test results

Connector	Ultimate Force (lbf)	Actuator Displacement (inches)	String Potentiometer Displacement (inches)
S6C15	6492	0.520	0.428
S6C16	7337	0.550	0.409
S7C17	9267	0.565	0.319
S7C18	10477	0.564	0.323
Averages	8393	0.550	0.369

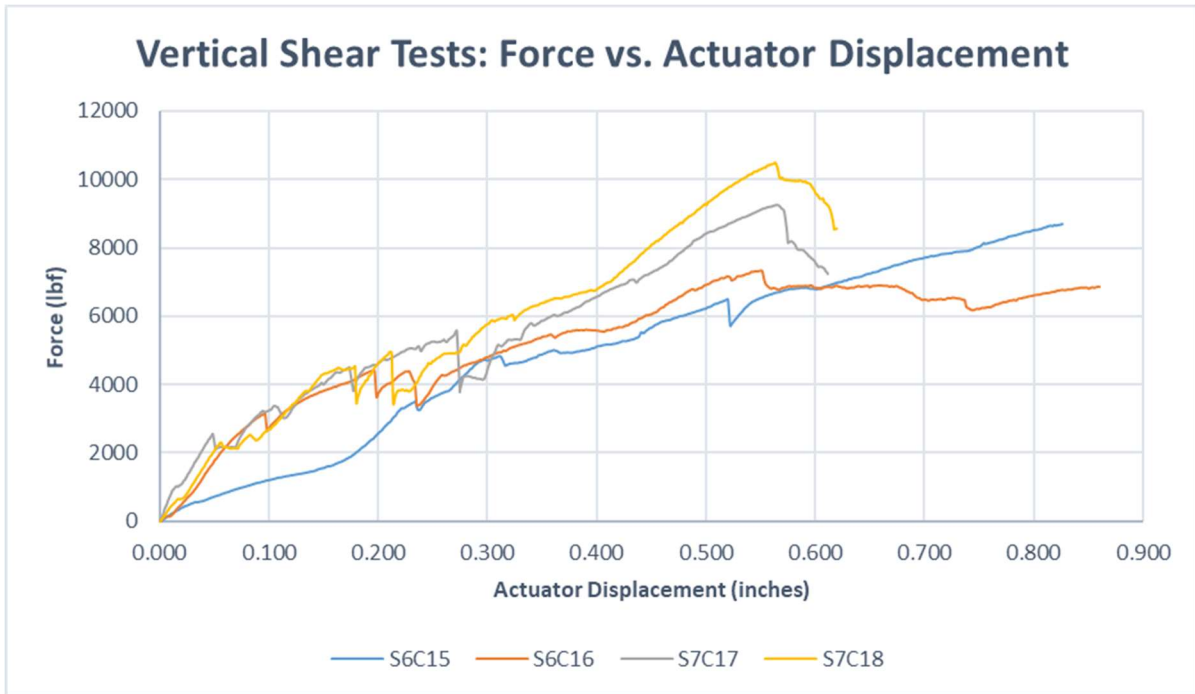


Figure 6.17. Vertical shear tests force versus actuator displacement

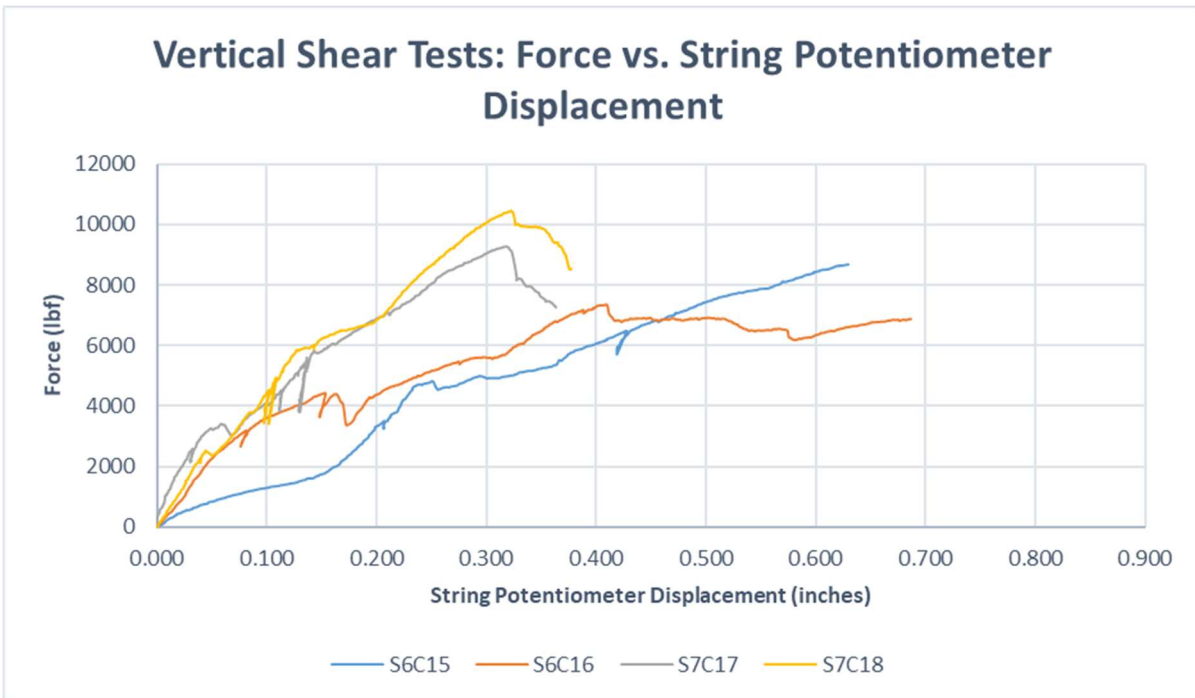


Figure 6.18. Vertical shear tests force versus string potentiometer displacement

The first vertical shear test was on the connector named S6C15. As the experiment was being conducted, the steel table that the slab was fixed to had begun to rotate about the feet nearest to where the load was applied. The test was stopped before ultimate load was achieved so the steel table could be secured to the Strong Floor as described in the test procedure. The slab was cracked when the test was stopped. The slab cracked perpendicular to the connector across the slab and diagonally on one side of the embedment, see Figure 6.19. The concrete under the embedment was cracked as well, see Figure 6.20. The slab cracked this way due to a gap between the bottom face of the slab and the table.

The other three vertical shear tests provided consistent data after the steel table was fixed in place. The average of the three tests recorded an ultimate force of 9,027 lbf, an actuator displacement of 0.560", and string potentiometer displacement of 0.350". When the specimens achieved their largest load, the slab around the connector cracked conically from the end of the embedment out the edge of the slab and is shown in Figure 6.21, Figure 6.22, and Figure 6.23. After the maximum load was obtained and the slab cracked, the load would not be regained because large gaps began propagating at the end of the connector's embedment as seen in Figure 6.24.



Figure 6.19. S6C15 cracking at the end of the test



Figure 6.20. S6C15 concrete cracked under the embedment



Figure 6.21. S7C17 cracking at failure



Figure 6.22. S6C16 cracking at failure



Figure 6.23. S7C17 cracking at failure



Figure 6.24. Typical large gaps in the cracks after failure for vertical shear tests

Cyclic Loading

Cyclic Horizontal Shear Test

The cyclic horizontal shear tests were the fourth type of test conducted in this research. The connectors that were tested were S5C14, S8C19, and S8C20. As previously mentioned, the loading protocol for this test involved two different displacement increment sizes based upon the monotonic horizontal shear test data. The purpose of the two increment sizes was to capture the bilinear load-displacement curve where the connector experiences elastic deformation in the first portion of the curve and strain hardening in the second portion. The results of linear-elastic deformation region are provided Table 6.6. The results at the start of strain hardening are provided in

Table 6.7. The actuator cycled three times for each increment of displacement which generated load-displacement hysteresis loops on the plots for each test. The data obtained from the cyclic tests was plotted on top of the monotonic horizontal shear displacement envelope developed from the shear tests for comparison. The plots for S5C14 are shown in Figure 6.25 and Figure 6.26. The plots for S8C19 are shown in Figure 6.27 and Figure 6.28. The plots for S8C20 are shown in Figure 6.29 and Figure 6.30.

Table 6.6. Monotonic and cyclic horizontal shear linear-elastic deformation

Linear-Elastic Region							
Monotonic Horizontal Shear				Cyclic Horizontal Shear			
Connector	Ultimate Force (lbf)	Actuator Disp. (inches)	String Pot. Disp. (inches)	Connector	Ultimate Force (lbf)	Actuator Disp. (inches)	String Pot. Disp. (inches)
S2C6	2020	0.059	0.039	-	-	-	-
S1C2	2418	0.155	0.095	S5C14	3464	0.172	0.100
S1C3	2941	0.125	0.109	S8C19	2852	0.148	0.115
S5C13	2922	0.174	0.147	S8C20	2383	0.123	0.111
Averages	2575	0.128	0.097	Averages	2900	0.148	0.109

Table 6.7. Monotonic and cyclic horizontal shear at the start of strain hardening region

Start of Strain Hardening Region							
Monotonic Horizontal Shear				Cyclic Horizontal Shear			
Connector	Ultimate Force (lbf)	Actuator Disp. (inches)	String Pot. Disp. (inches)	Connector	Ultimate Force (lbf)	Actuator Disp. (inches)	String Pot. Disp. (inches)
S2C6	4066	0.431	0.273	-	-	-	-
S1C2	3425	0.368	0.262	S5C14	4205	0.246	0.165
S1C3	3483	0.197	0.174	S8C19	3178	0.192	0.158
S5C13	3868	0.290	0.251	S8C20	2715	0.168	0.156
Averages	3710	0.322	0.240	Averages	3366	0.202	0.160

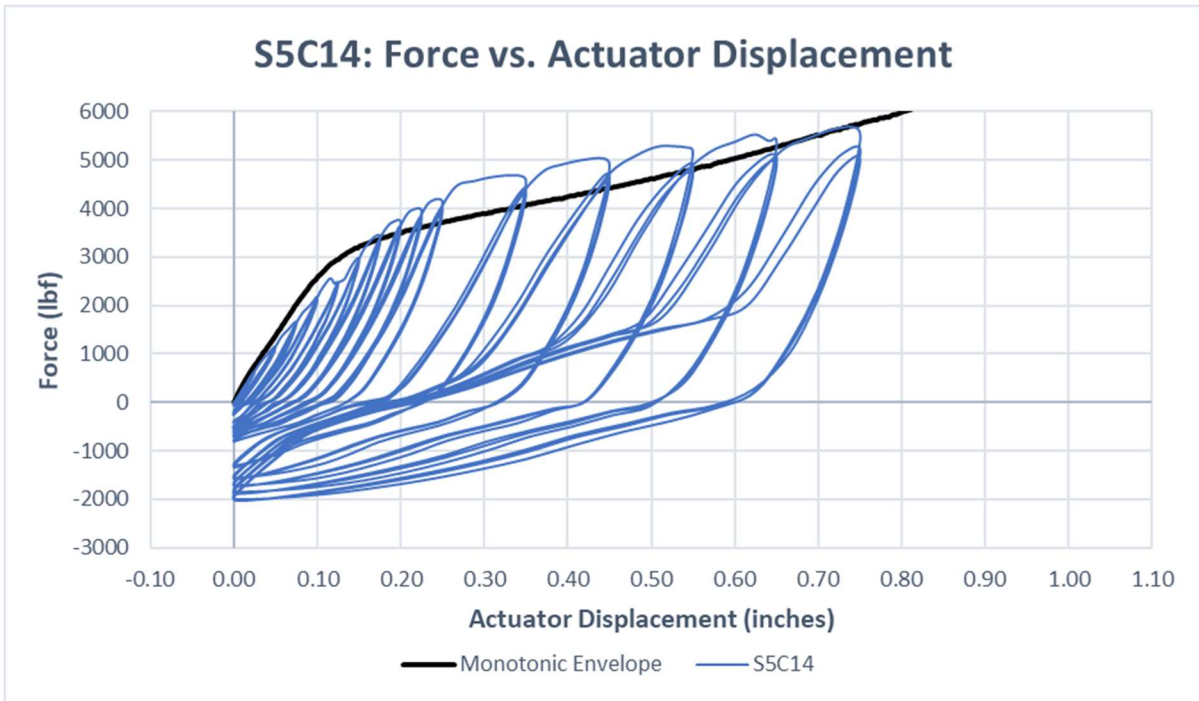


Figure 6.25. S5C14 force versus actuator displacement plot

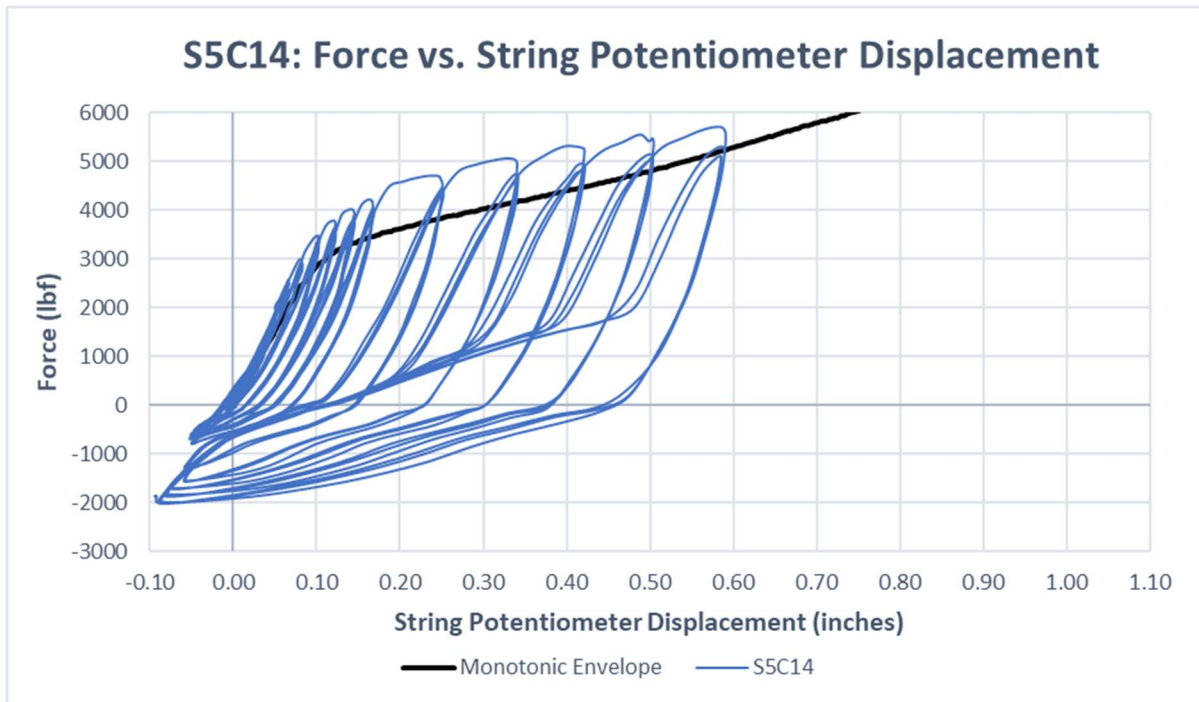


Figure 6.26. S5C14 force versus string potentiometer displacement plot

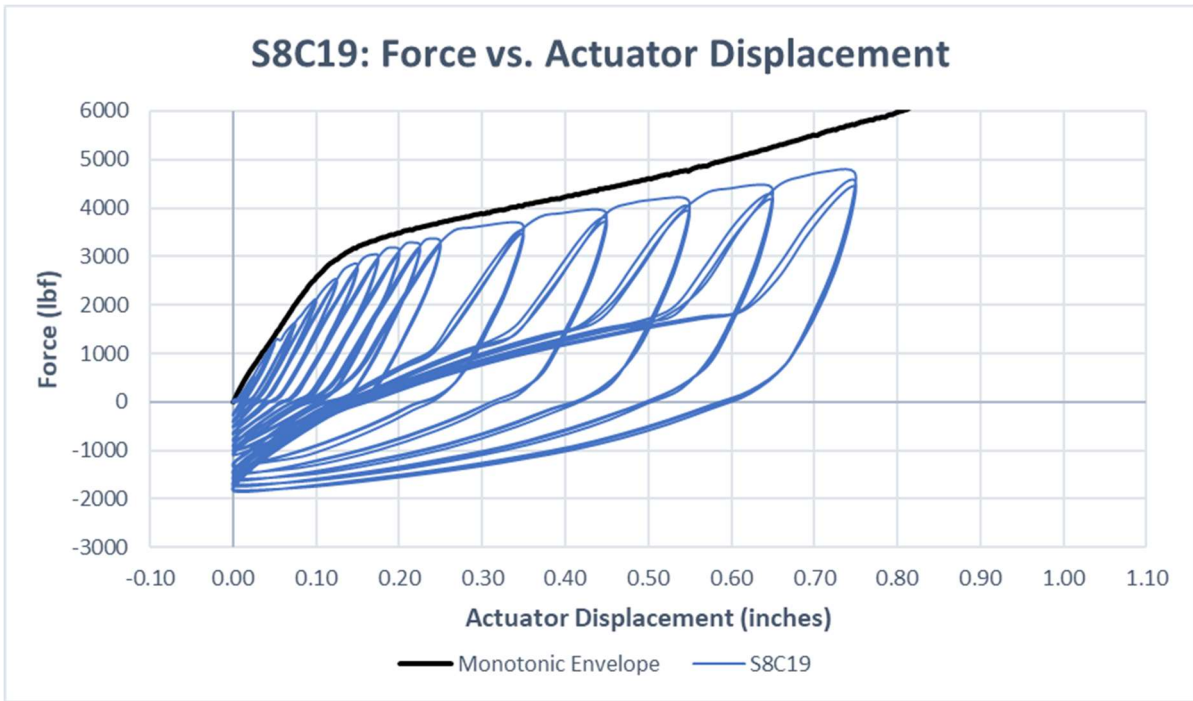


Figure 6.27. S8C19 force versus actuator displacement plot

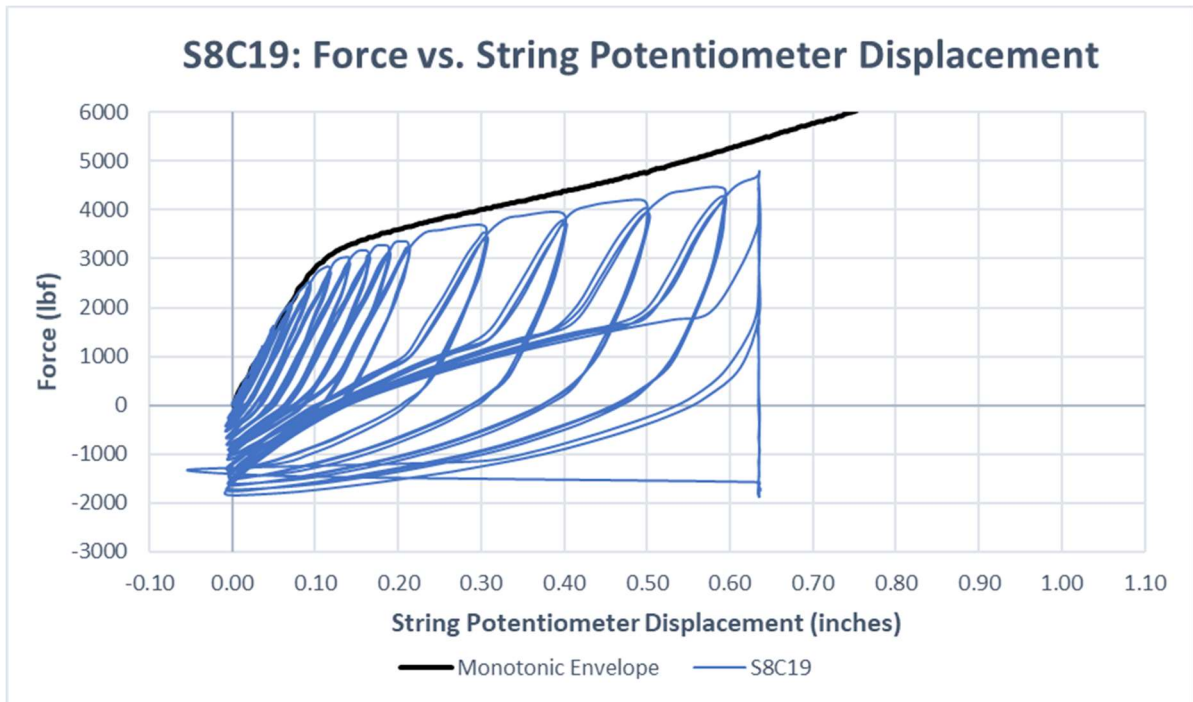


Figure 6.28. S8C19 force versus string potentiometer displacement plot

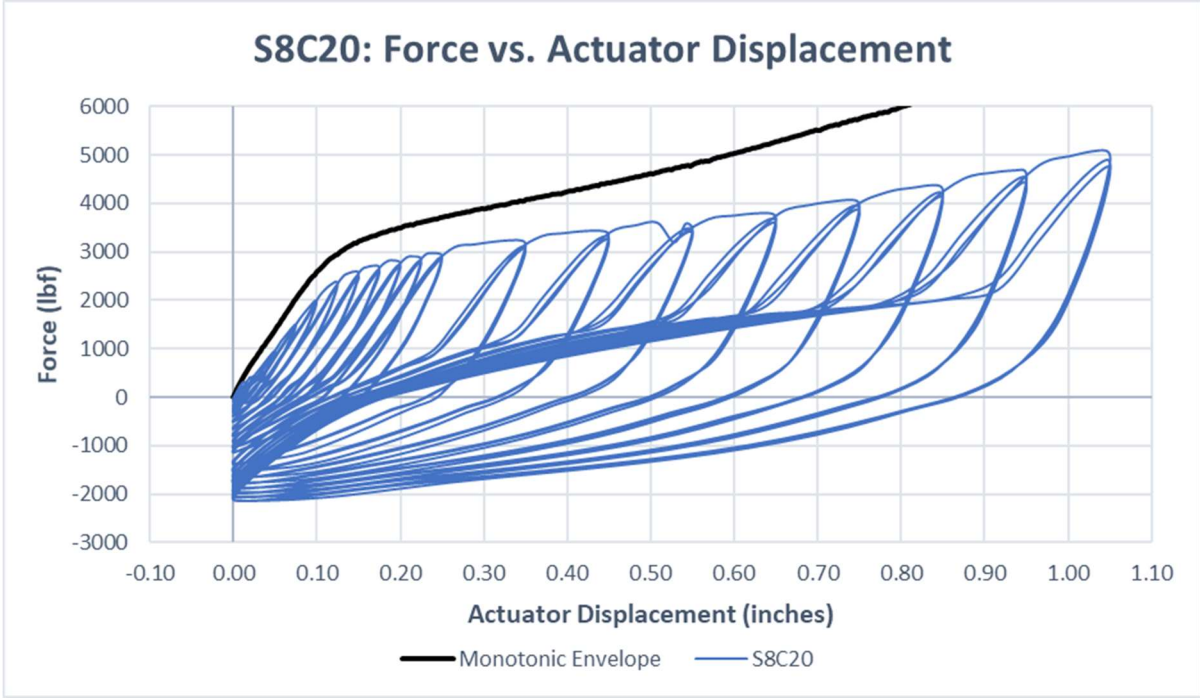


Figure 6.29. S8C20 force versus actuator displacement plot

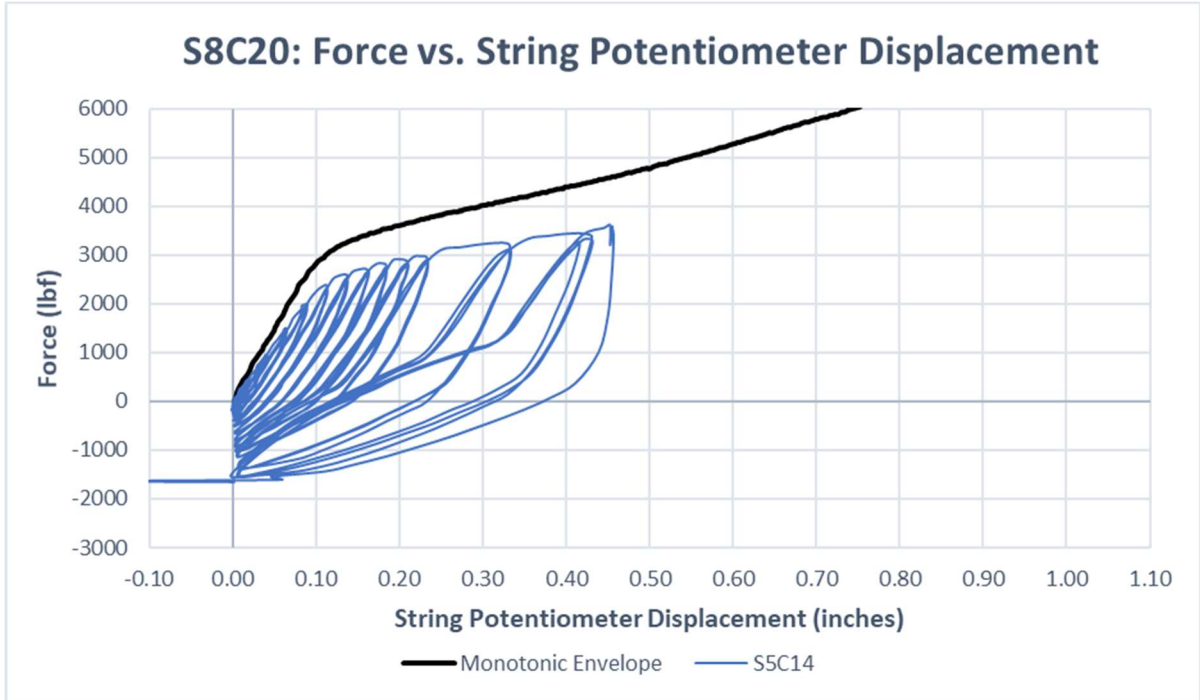


Figure 6.30. S8C20 force versus string potentiometer displacement plot

The plots generated from the cyclic horizontal shear test data were nearly identical in shape and were within the monotonic tests load-displacement envelope, except for S5C14 which achieved a higher load, initially. During the displacement cycles from 0 to 0.125 inches the slope of the load-displacement plots was a steep linear relationship during loading and then slightly concave up during unloading. In this region, the connector experienced linear-elastic deformation. The connectors became deformed from increasing displacement which produced a negative force in the system as the actuator returned to zero due to the permanent deformation induced. The negative force increased as the displacement was increased, but it was not a linear relationship. When the connector was displaced after 0.125 inches it entered the strain hardening region of the plot, which was a less steep linear relationship of stiffness, and the connector begins to rotate at its embedment, shown in Figure 6.31. The displacement steps in the strain hardening region have two levels of stiffness where the initial stiffness of the first cycle nearly matches the secondary stiffness of previous step's second and third cycle. There was no failure mode present during the tests due to elongation of the stainless-steel, which was also observed in monotonic tests. When the load was removed from the connector after the test, the permanent deformation was visible, see Figure 6.32.



Figure 6.31. Typical cyclic horizontal shear connector with an applied load



Figure 6.32. Typical cyclic horizontal shear connector permanently deformed after testing

Cyclic Vertical Shear Test

The cyclic vertical shear test was the fifth test type conducted in this research and the connectors that were tested were S3C8, S3C9, S4C11, and S4C12. The displacement cycles of the actuator produced load-displacement hysteresis loops which were plotted on top of the

monotonic vertical shear test displacement envelope. The plots for S3C8 are provided in Figure 6.33 and Figure 6.34. The plots for S3C9 are provided in Figure 6.35 and Figure 6.36. The plots for S4C11 are provided in Figure 6.37 and Figure 6.38. The plots for S4C12 are provided in Figure 6.39 and Figure 6.40. The ultimate force and displacements for the cyclic test is provided next to the monotonic results in Table 6.8.

Table 6.8. Monotonic and cyclic vertical shear test results

Monotonic Vertical Shear Results				Cyclic Vertical Shear Results			
Connector	Ultimate Force (lbf)	Actuator Disp. (inches)	String Pot. Disp. (inches)	Connector	Ultimate Force (lbf)	Actuator Disp. (inches)	String Pot. Disp. (inches)
S6C15	6492	0.520	0.428	S3C8	3346	0.247	0.207
S6C16	7337	0.550	0.409	S3C9	9464	0.699	0.586
S7C17	9267	0.565	0.319	S4C11	8016	0.499	0.312
S7C18	10477	0.564	0.323	S4C12	5898	0.221	0.149
Averages	8393	0.550	0.369	Averages	6681	0.416	0.313

The load versus displacement plots for the cyclic vertical shear tests provided varying results for each test, however they did not exceed the ultimate load obtained in the monotonic tests. The cyclic tests did not experience as many drops in load throughout the tests as the monotonic test data showed. Two failure modes occurred during the tests. The primary failure mode was due to concrete cracking conically from the end of the connector’s embedment to the edge of the slab, which occurred in the tests of S3C9, S4C11, and S4C12 and is shown in Figure 6.41, Figure 6.42, and Figure 6.43, respectively. Connector S3C8 failed by the connector punching through the bottom of the slab, see Figure 6.44 and Figure 6.45, which occurred due to a gap between the table and the uneven surface on the bottom of the slab.

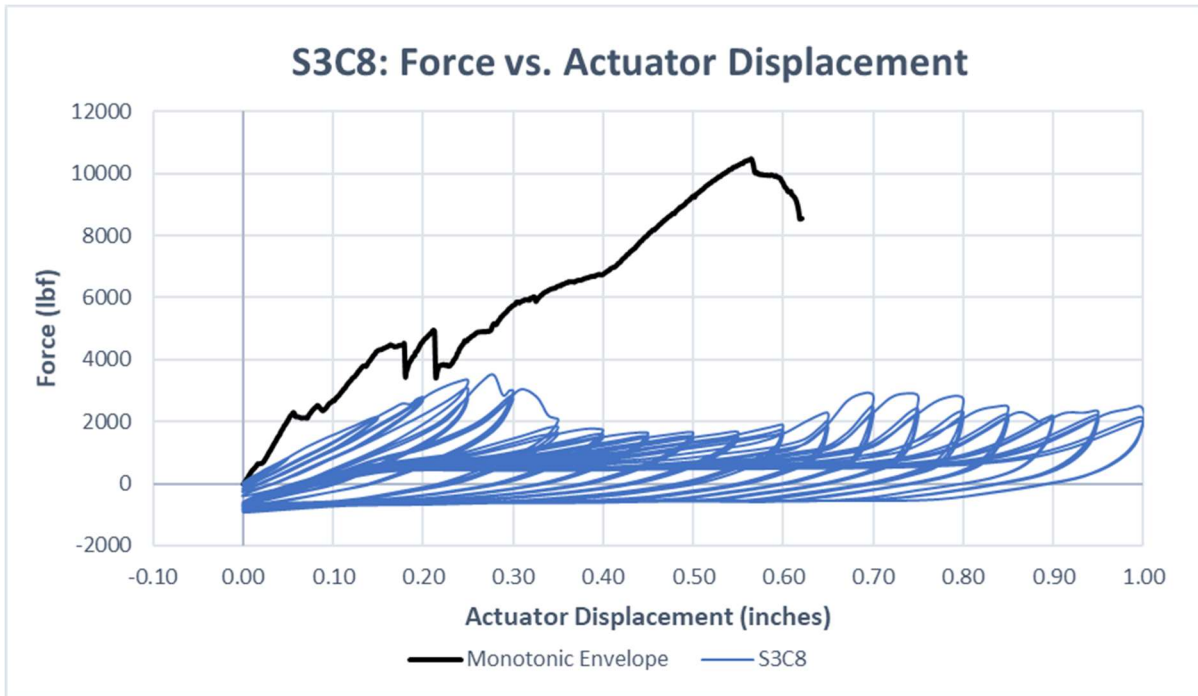


Figure 6.33. S3C8 force versus actuator displacement plot

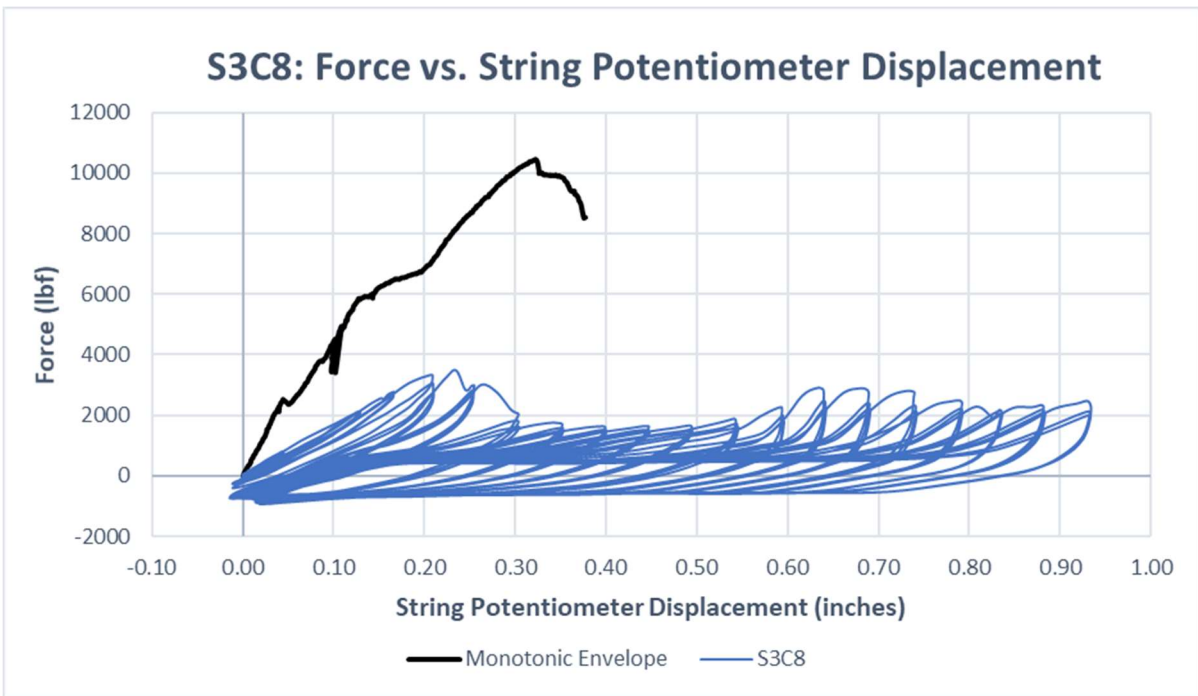


Figure 6.34. S3C8 force versus string potentiometer displacement plot

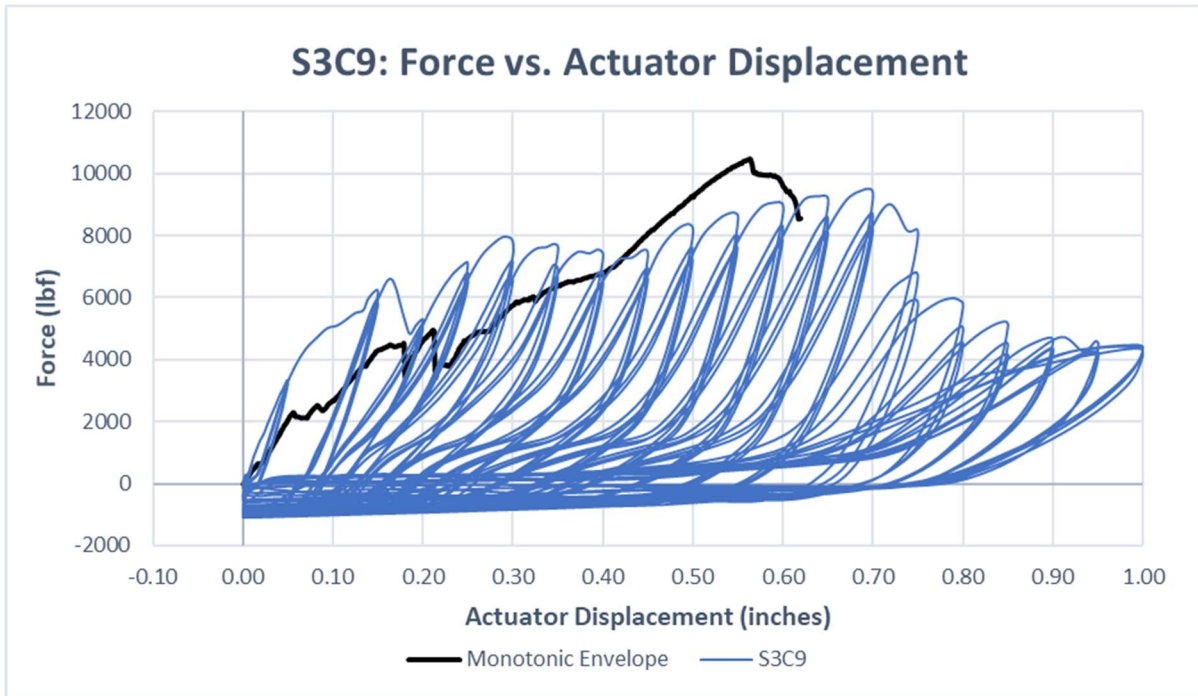


Figure 6.35. S3C9 force versus actuator displacement plot

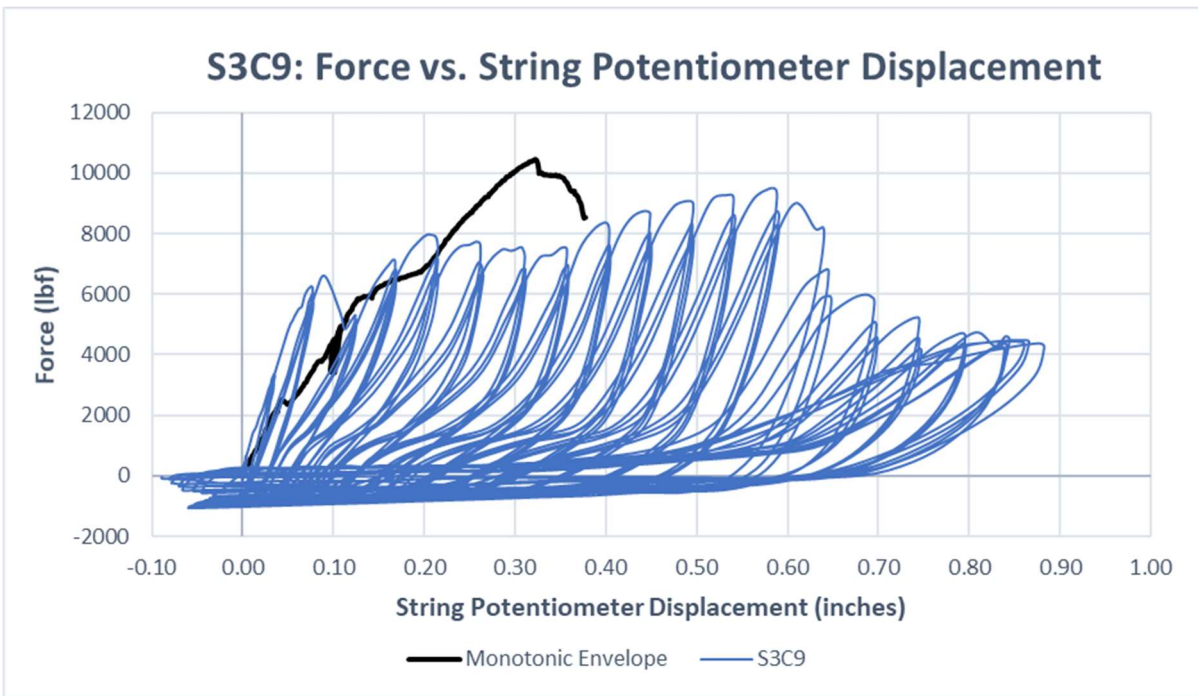


Figure 6.36. S3C9 force versus string potentiometer displacement plot

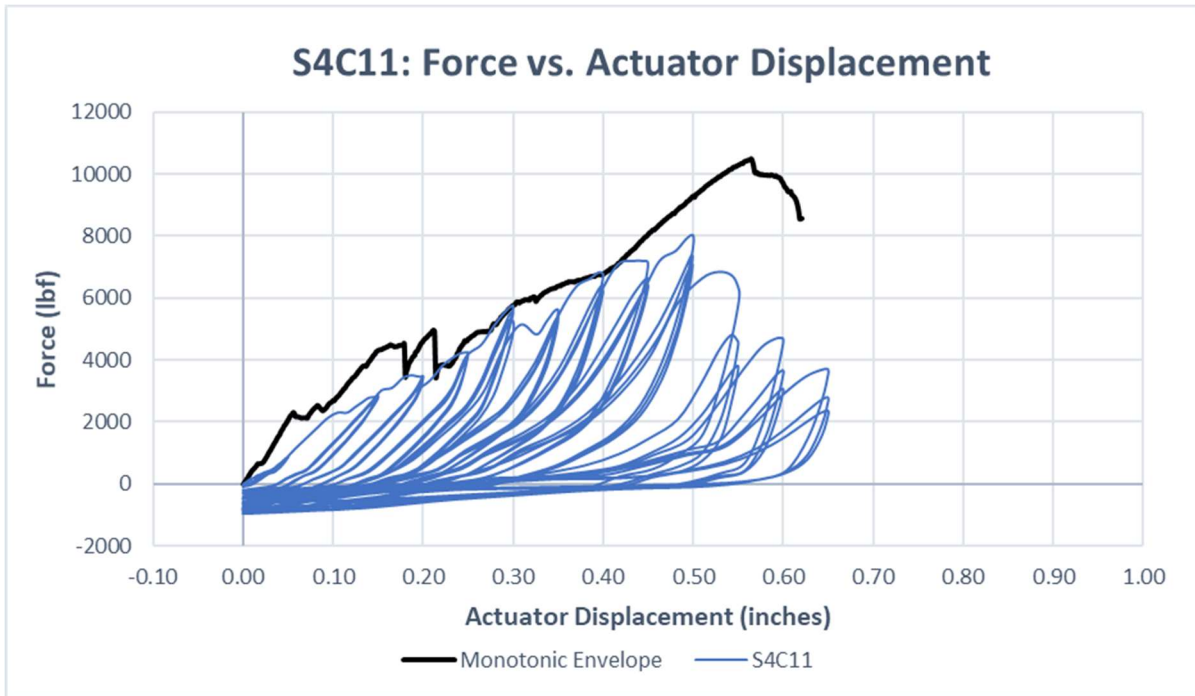


Figure 6.37. S4C11 force versus actuator displacement plot

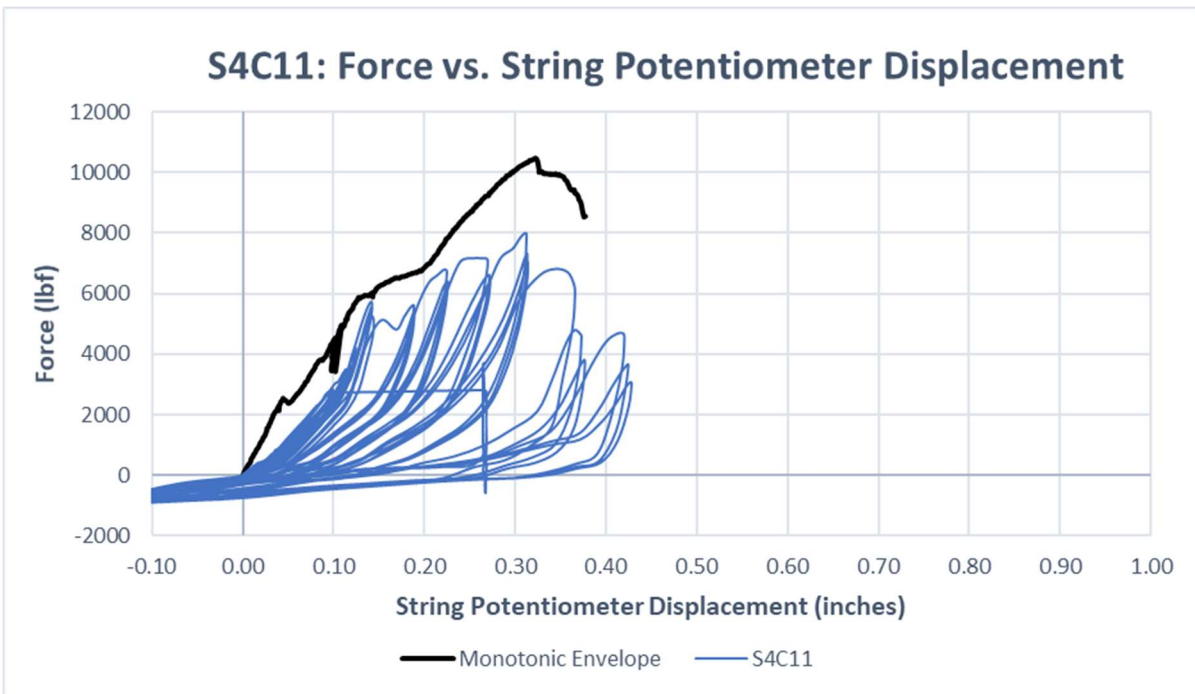


Figure 6.38. S4C11 force versus string potentiometer displacement plot

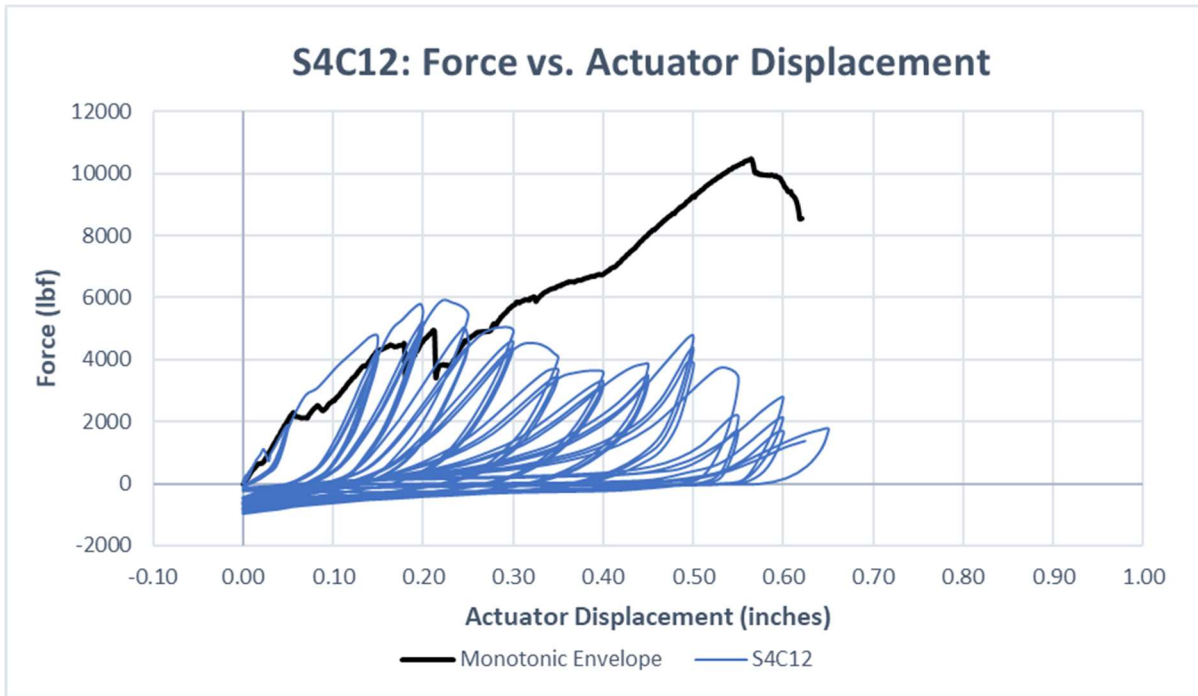


Figure 6.39. S4C12 force versus actuator displacement plot

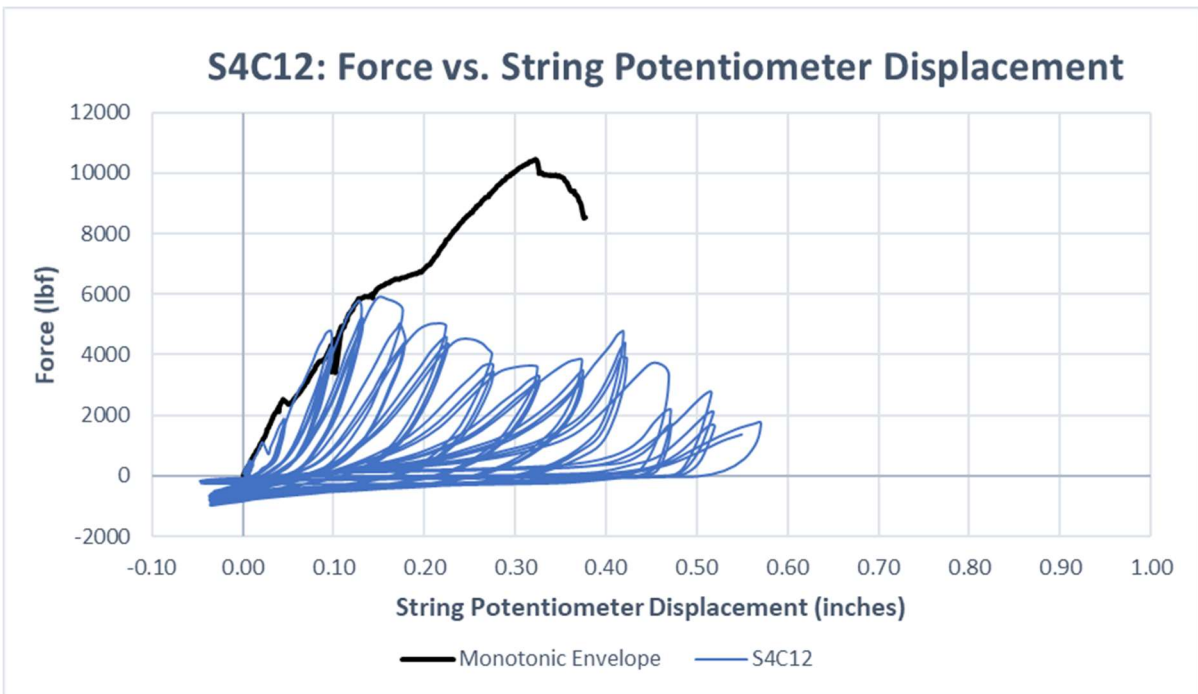


Figure 6.40. S4C12 force versus string potentiometer displacement plot



Figure 6.41. S3C9 failure



Figure 6.42. S4C11 failure



Figure 6.43. S4C12 failure

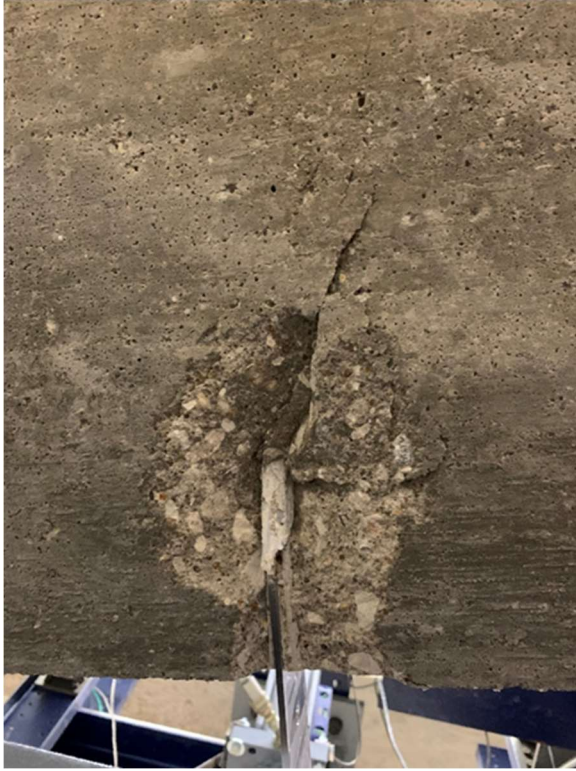


Figure 6.44. S3C8 failure on the bottom face



Figure 6.45. S3C8 failure (slab edge view)

The test on S3C8 began to break through the bottom when the connector was displaced 0.278 inches with a load of approximately 3,500 lbf. The test was not stopped to see if the load would rise again, which it did on the first cycle at 0.700 inches of displacement. The likely cause of the connector regaining strength was from it bearing on the testing table. The connector's embedment remained to have strength after it started to break through the slab. The maintained strength was attributed to the narrowing height of the connector at the end of the embedment and friction forces between the epoxy and the connector's rough surface. The force on the connector did not fall below 1,500 lbf anytime during the test, except when the actuator cycled back up.

Connector S3C9 obtained the highest load of the cyclic vertical shear tests which was approximately 9,500 lbf on the first cycle of 0.700 inches. Connector S3C9 had the stiffest response of the cyclic vertical shear tests and was outside of the monotonic load-displacement envelope through the first 0.500 inches of displacement cycles. The first crack appeared on the

first cycle of 0.200 inches, which caused the load to drop. The load was regained on the next displacement step. The load was maintained until the cracks began to propagate after 0.700 inches. When the loading protocol was finished, the connector's embedment was completely separated from the slab and was able to be removed by hand, see Figure 6.46. The epoxy debonded on most of one side of the connector and the roughed surface of the connector was exposed, see Figure 6.47.



Figure 6.46. S3C9 separated connector



Figure 6.47. S3C9 debonded epoxy

Connector S4C11 produced results that were most like the monotonic tests with an ultimate load of approximately 8,000 lbf at a displacement of 0.500 inches. The load-displacement plot followed the monotonic test envelope until the embedment failed on the first cycle of 0.550 inches, which was approximately when the monotonic tests failed. The test was stopped shortly after failure because the embedment was completely separated. When the slab

was removed from the testing table the concrete surrounding the embedment was removed by hand and the rebar wire mesh was exposed, see Figure 6.48 and Figure 6.49.

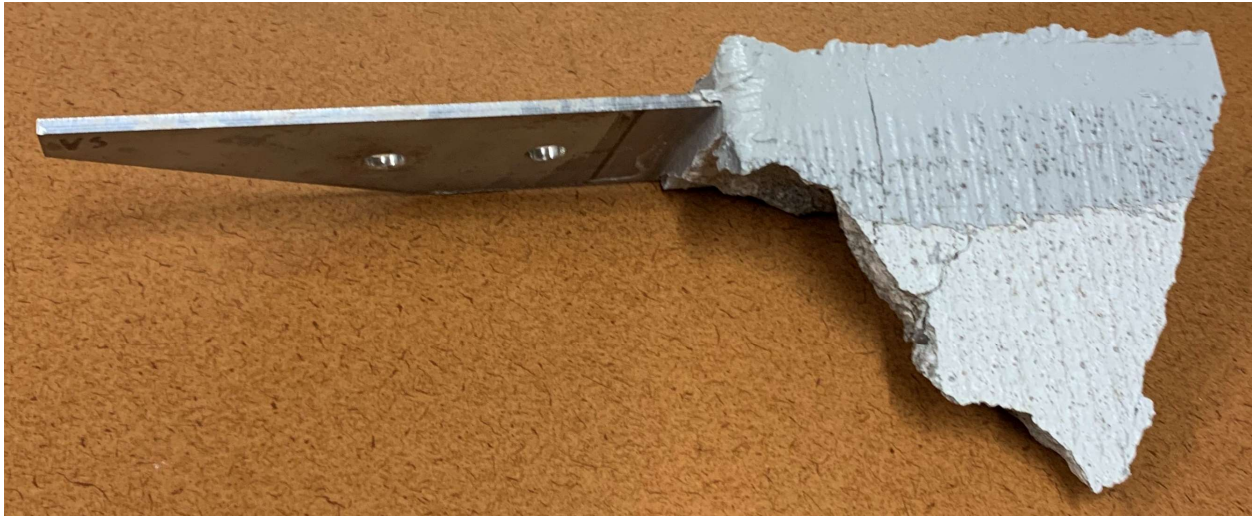


Figure 6.48. S4C11 separated connector



Figure 6.49. S4C11 spalled embedment and exposed wire mesh rebar

Connector S4C12 recorded the lowest ultimate load of the cyclic vertical shear tests at approximately 5,900 lbf at a displacement of 0.221 inches. The load-displacement plot exceeded the monotonic envelope by approximately 1,000 lbf from 0.100 inches to 0.250 inches. The embedment first cracked when the ultimate load of the test was achieved. The same failure mode as S3C9 and S4C11 was observed in this test, but the embedment remained connected with the slab after the test was stopped.

Flexural Test

The flexural test was the sixth test type conducted in this research and only one test was performed with two slabs adjoined by one connector for this test type. As previously mentioned in the Flexural Test Experimental Program section of this paper, S8 and S9 were the two slabs used for the test. Actuator displacement was recorded but was not used to generate a plot because the actuator was not where the force was applied on the specimen. The force on the connector was calculated from the applied actuator force. It was used to create a force versus string potentiometer displacement plot which is shown in Figure 6.50. The force-displacement plot can be approximated into three regions of stiffness: first slab yielding, second slab yielding, and ultimate failure of the system. The maximum values for each region were recorded in Table 6.9. The yielding of the slabs was assumed to be when each slab cracked. The assumption was justified because the steel reinforcement in the slabs was not adequate to support a cracked concrete section and is not the typical reinforcement in precast double-tee concrete beams.

Table 6.9. Flexural test results

Region	Force (lbf)	Displacement (inches)
First Slab Yielding	6258	0.039
Second Slab Yielding	9333	0.135
Ultimate Failure	8717	0.663

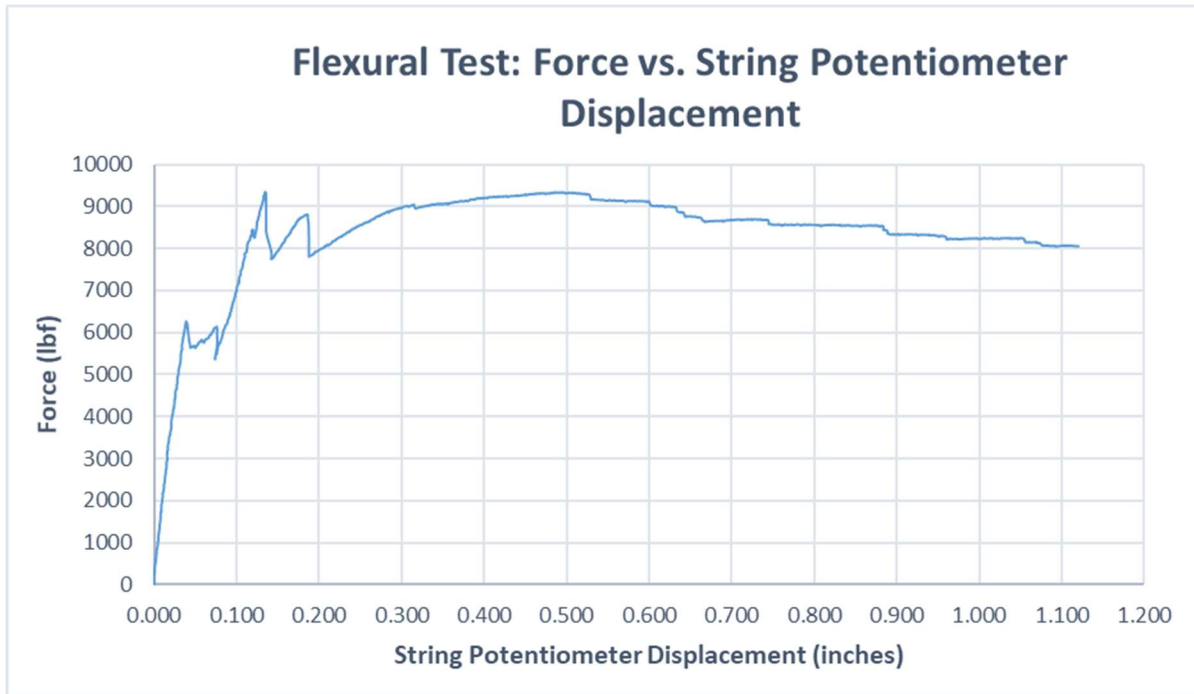


Figure 6.50. Flexure test force versus string potentiometer displacement

The first stiffness region was when the system underwent linear-elastic deformation until the first slab yielded. The first slab that yielded was S9, which had the load applied on it. It is shown in Figure 6.51. When S9 cracked, the load dropped about 600 lbf and the cantilevered span of the slab began to rotate about the edge of the steel table that the slab was fixed to. The load remained stable between 5,500 lbf and 6,100 lbf while the slab rotated. Once a critical amount of rotation occurred in S9, the uncracked stiffness of the second slab allowed the load to increase in the second load-displacement stiffness region until the slab yielded. The second stiffness region was linear but was less steep than the first region. The different stiffnesses occurred in the system because S9 was allowed to rotate more, being yielded. When S8 cracked it dropped the load and both slabs began to rotate, see Figure 6.52. The third region was when the system ultimately failed. The ultimate failure region exhibited a nonlinear concave stiffness. The load reached a maximum force of 9,329 lbf at 0.487 inches of displacement during the nonlinear stiffness response of the system. The system experienced significantly more

deformation in this region than the first two regions which caused the slabs to be noticeably rotated, see Figure 6.53. When the test was stopped, the slab's steel reinforcement and the connector held the cantilevered spans to the part of the slab that was fixed to the tables. Figure 6.54 shows the slabs after they have been tested.

Cracks appeared on the top face and edges of the slabs shortly before they yielded. The first cracks were on the face of the slabs above the edges of the tables at the start of the cantilevered span. Diagonal cracks formed on the slab edges that started at the edge of the table and proceeded away from the applied load where they connected to the face cracks, see Figure 6.55. S8 cracked at the same distance from the embedment as S9 on the face of the slab, but the cracks on the edges of the slab cracked along the embedment of the connectors that were tested previously, see Figure 6.56. There was no cracking anywhere else on the specimen when the test was concluded. The connector's embedment in the two slabs had separated from the epoxy on the bottom of the embedment, see Figure 6.57, but the top surface of the embedment was still intact. The connector was permanently deformed from the test but did not show signs of rupture.

The flexural test provided sufficient results to prove that a system of precast concrete cantilevers adjoined with a connector have sufficient strength to resist typical loads from vehicles. The ductility of connector allowed for significant reserved flexural strength under a large deformation. The strength observed in the system is particularly noteworthy considering the lack of steel reinforcement in the concrete section.



Figure 6.51. S9 cracked at yielding



Figure 6.52. S8 cracked at ultimate yielding



Figure 6.53. Slab rotations after flexural test



Figure 6.54. Top view of the slabs after the flexural test



Figure 6.55. S9 face and edge cracks



Figure 6.56. S8 face and edge cracks



Figure 6.57. Embedment crack after the flexural test

Chapter 7 - Modeling and Design Equations

The models developed to supplement the experimental results of this research were developed from two structural analysis theories. The two theories used were the modified compression field theory (MCFT) and the plastic hinge theory. Four models were constructed from these theories based upon experimental observations of crack patterns, failure modes, and specimen deformations. The analyses for the models took the steel reinforcement in the slabs into consideration, which is not the typical reinforcement found in precast double-tee concrete beams. The results of the models support the strengths observed in the experimental tests conducted.

The modified compression field theory is a method of analysis that is used to predict the axial and shear forces in reinforced concrete members. The MCFT uses the relationship of stresses, strains, angle of cracks, and spacing of cracks to calculate the forces in concrete members. The MCFT was used to produce an axial tension model and a vertical shear model to analyze the strength of the connector and its embedment.

Plastic hinge theory is a method of stiffness analysis that is used to analyze structural members that have surpassed their initial elastic stiffness and have begun to plastically deform. The analysis of plastic hinges is typically performed on nonlinear materials that experience significant deformation without fracturing. The plastic hinge theory was used to develop the horizontal shear model and the flexural model.

Axial Tension Model

The developed axial tension model used the axial strength calculations from the modified compression field theory to predict the ultimate axial strength capacity of the connector. The model used a convergence analysis of axial strength. The model assumed that area of the steel,

A_s , in tension was located at the tip of the connector's embedment, which is where the axial tension tests first cracked. The effective width of the section, d_v , that resisted the applied axial force was assumed at the center of the depth of the embedded connector. Figure 7.1 provides the detailing for the axial tension model. The general parameters used in the axial tension model are provided in Table 7.1.

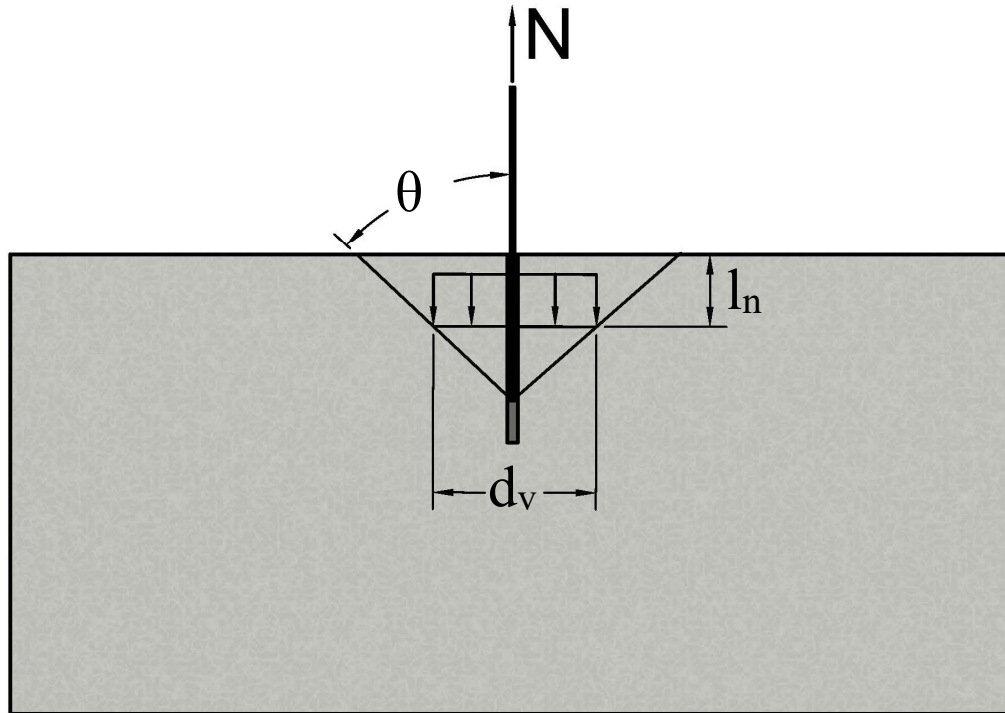


Figure 7.1. Axial tension model diagram

Table 7.1. General Parameters for the Axial Tension Model

Parameter	Value	Units
E_s	29000	ksi
A_s	0.14	inches ²
f'_c	4.85	ksi
l_n	3.50	inches
h	4.00	inches

The first step in the model was to estimate an initial axial force, N_i , applied on the connector. The estimated axial force in the steel was used to calculate the strain in the steel, ε_s , from the stiffness of the connector with Equation 7.1. The angle of the crack, θ , at the tip of the embedment was calculated with Equation 7.2 using the steel strain and was used to find the effective width of the section with Equation 7.3. The resultant axial tension force, N_R , was then calculated with Equation 7.4. The last step was to take the difference in the resultant force from the initial axial force. The Goal Seek function in Excel was used to find the initial axial force that would converge the difference of forces to zero. The results of the model are provided in Table 7.2.

Equation 7.1 . Strain in the steel for the axial tension model

$$\varepsilon_s = \frac{N}{E_s A_s}$$

Equation 7.2. Angle of crack for the axial tension model

$$\theta = 29 + 7000\varepsilon_s$$

Equation 7.3. Effective width of the section for the axial tension model

$$d_v = 2l_n \tan(\theta)$$

Equation 7.4. Resultant axial tension force

$$N_R = 5.35\sqrt{f'_c}hd_v/1000$$

Table 7.2. Axial Tension Model Results

Calculation	Initial Iteration	Convergence Iteration
N_i (lbs)	13000	13144
ϵ_s	0.00319	0.00322
θ (degrees)	51.31	51.56
d_v (inches)	8.74	8.82
N_R (lbs)	13028	13144
$N_R - N_i$	28	0

Vertical Shear Model

The generated vertical shear model used an iterative step process to calculate the ultimate shear capacity of the connector. The model assumed that cracks would originate diagonally at 45 degrees from the end of the connector's embedment and that the initial effective width, b_w , of the concrete in shear was at the middle of the embedment length. The depth of the steel reinforcement, d , was 1.75 inches, which was half the height of the connector with the additional 0.25 inches from face of the slab. The effective depth of the section, d_v , was calculated to be 72% of the height of the section, h . The detailing for the vertical shear model is provided in Figure 7.2 and Figure 7.3. The general parameters for the model are provided in Table 7.3.

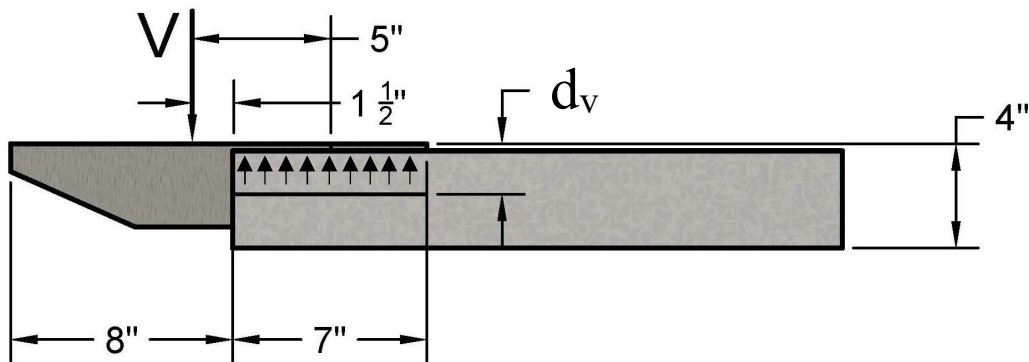


Figure 7.2. Vertical shear model side view diagram

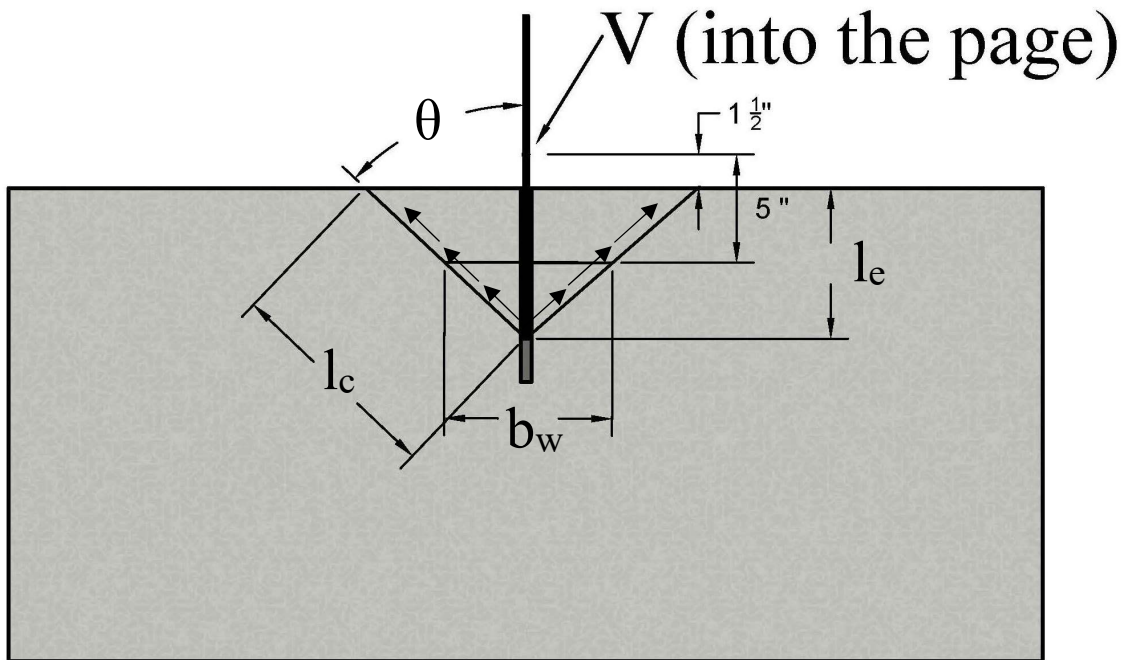


Figure 7.3. Vertical shear model top view diagram

Table 7.3. General parameters for the vertical shear model

Parameter	Value	Units
f'_c	4.85	ksi
f_y	51.50	ksi
b_w	7.00	inches
d	1.75	inches
h	4	inches
d_v	2.88	inches
A_s	0.5625	inches ²

The connector was modeled as a cantilevered beam from the slab with the simulated load applied 1.5 inches from the edge of the slab. The first step of the iterative analysis calculated the shear concrete force, V_c , according to the shear concrete force in Equation 7.5 from the ACI 318-19. This initial force provided an estimated starting point with which to iterate the model. The

concrete force was then used to calculate the internal moment, M , from the applied load at a distance of 5 inches away with Equation 7.6. The strain in the steel was then calculated from the shear force and the moments, in Equation 7.7. The angle of the crack, θ , was calculated with Equation 7.8 and was used to find the total length of the crack developed at failure in Equation 7.9. The beta value, β , was calculated in Equation 7.10. The final step of the iteration calculated the resultant vertical shear force with Equation 7.11, and was used as the initial shear force in the second iteration. These steps were repeated until iterations converged. The results of the vertical shear model are provided in Table 7.4.

Equation 7.5. Shear concrete force (ACI 318-19 Equation 22.5.5.1a)

$$V_c = 2\sqrt{f'_c}b_w d$$

Equation 7.6. Internal moment

$$M = 5V_c$$

Equation 7.7. Strain in steel for the vertical shear model

$$\varepsilon_s = \frac{1}{2} \frac{V + M/d_v}{E_s A_s}$$

Equation 7.8. Angle of crack for the vertical shear model

$$\theta = 29 + 3500\varepsilon_s$$

Equation 7.9. Crack length

$$l_c = 2 \frac{l_e}{\cos\theta}$$

Equation 7.10. Beta value

$$\beta = \frac{4.8}{(1 + 750\varepsilon_s)}$$

Equation 7.11. Shear force in the concrete

$$V_c = 0.0316\beta\sqrt{f'_c}l_c d_v$$

Table 7.4. Vertical shear model results

Calculation	Iteration 1	Iteration 2	Iteration 3	Iteration 4	Iteration 5	Iteration 6
V_c (kips)	4.83	11.98	9.11	10.06	9.72	9.84
M (kip-in.)	24.13	59.91	45.54	50.31	48.61	49.20
ε_s	0.00040	0.00100	0.00076	0.00084	0.00082	0.00083
θ (degrees)	30.42	32.52	31.67	31.95	31.85	31.89
l_c (inches)	16.23	16.60	16.45	16.50	16.48	16.49
β	3.68	2.74	3.05	2.94	2.98	2.96
V_c (kips)	11.98	9.11	10.06	9.72	9.84	9.80

Horizontal Shear Model

The horizontal shear model was developed from a plastic nonlinear secant stiffness analysis. The load-displacement responses observed during the experimental tests provided that the connector plastically deformed and experienced strain hardening. The connector was modeled as a beam with fixed-pinned boundary conditions determined from the deformation and rotation that occurred during the experimental tests. The fixed support was at the connector's embedment in the slab and the pinned support was where the connector was attached to the test fixture. The plastic analysis captures the linear-elastic stiffness of the connector when the elastic moment of the connector's cross-section was reached. The elastic moment occurred when the extreme fibers of the cross-section yielded. To further analyze the plasticity of the cross-section, the connector was divided into 100 layers of thickness to observe moment-curvature relationship progress from the extreme fiber down to the centroid of the connector. The horizontal shear model only analyzed 50 layers due to the stress profile being symmetric. The model was incremented 50 times where each increment lowered the distance to the yielded layer. The strain hardening of the connector was adjusted in the stiffness for the layers that had already yielded. As each layer yielded, the moment-curvature relationship increased nonlinearly until the plastic moment of the cross-section was reached, see Figure 7.4. The reaction stiffnesses of a fixed-pinned beam was used to calculate the load and displacement from the moment curvature relationship. The calculated loads and displacements were plotted on the force versus string potentiometer displacements of the monotonic horizontal shear tests and is provided in Figure 7.5.

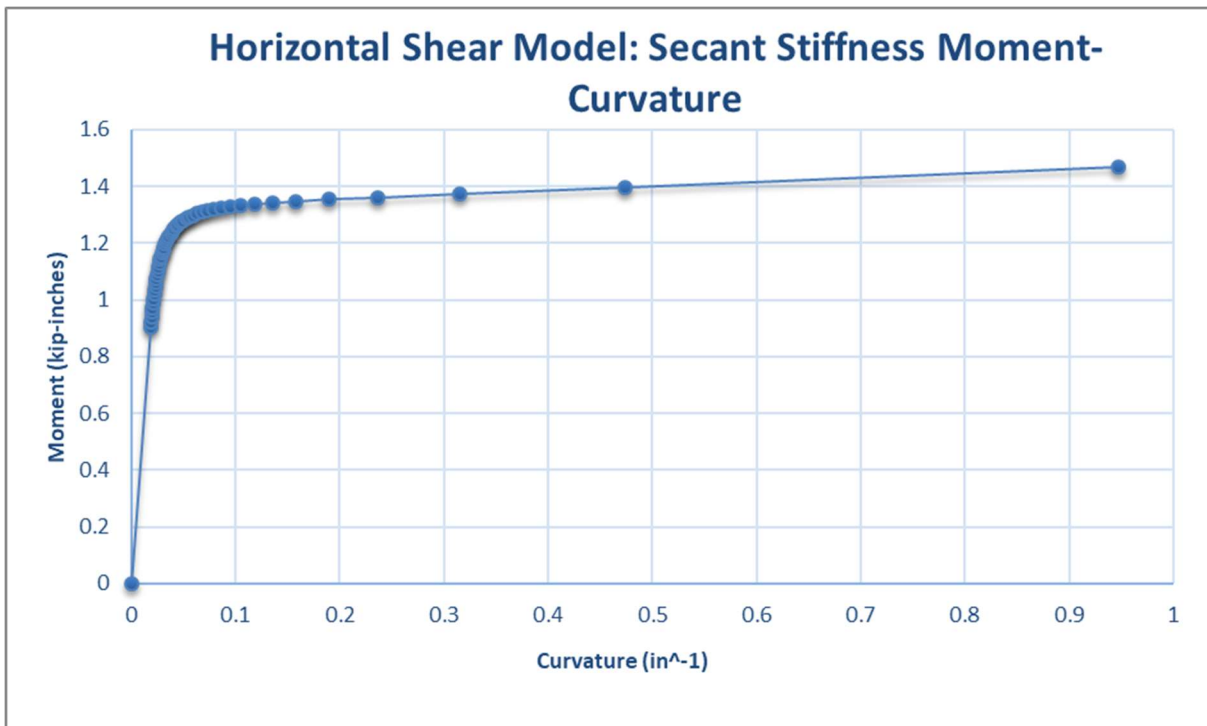


Figure 7.4. Horizontal Shear Model: Secant stiffness moment-curvature plot

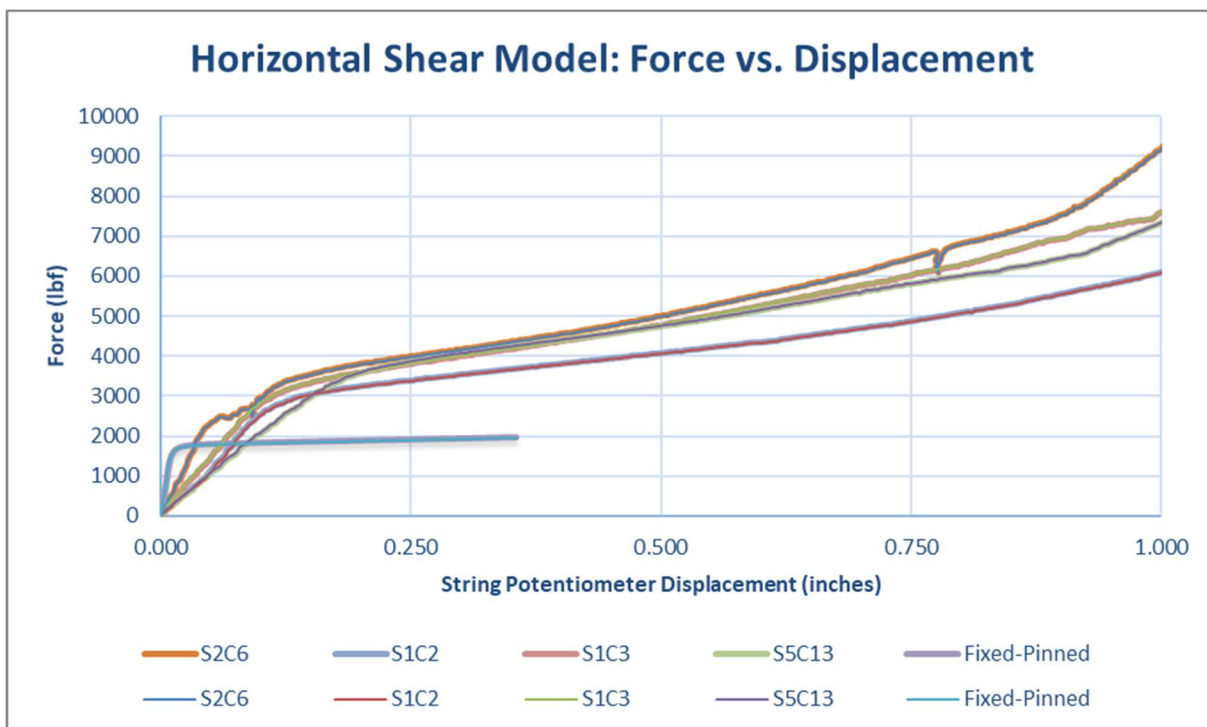


Figure 7.5. Horizontal shear model force versus displacement plot

Flexural Model

The flexural model was developed from the assumption of three plastic hinges forming based upon experimental observations. The first plastic hinge formed in the S9 slab, which had the load applied on it, at the fixed support. The second plastic hinge formed at the fixity of S8 slab. The third plastic hinge was assumed to be at the embedment of the connector in S9 of slab end. The three hinges are shown in Figure 7.6. The three plastic hinges were modeled using a two-dimensional matrix stiffness analysis to predict the load that was applied when each hinge formed. Two analyses were modeled to most accurately attempt to track the load-displacement curve of the experimental test. The two analyses assumed different effective moments of inertia for the slab sections. The load was applied transversely to a 14-inch wide roller of the slab during the flexural experiment, so it was assumed that the full width of the slab was not fully effective. The analyses are referred to as the half-width analysis and tapered analysis. The effective width for the half-width analysis was assumed to be half of the slab's width of 24 inches. The half-width assumption is constant for both slabs and was modeled with five nodes, see Figure 7.7. The tapered analysis assumed the effective width increased towards the fixed supports of each slab. The tapered analysis divided the cantilevered system into a total of 12 nodes separated with varying lengths shown in Figure 7.8. The moments of inertia were calculated in the middle of the links throughout the system, see Figure 7.9. The cracked moment of inertia was assumed to be at the link connected to the fixed support.

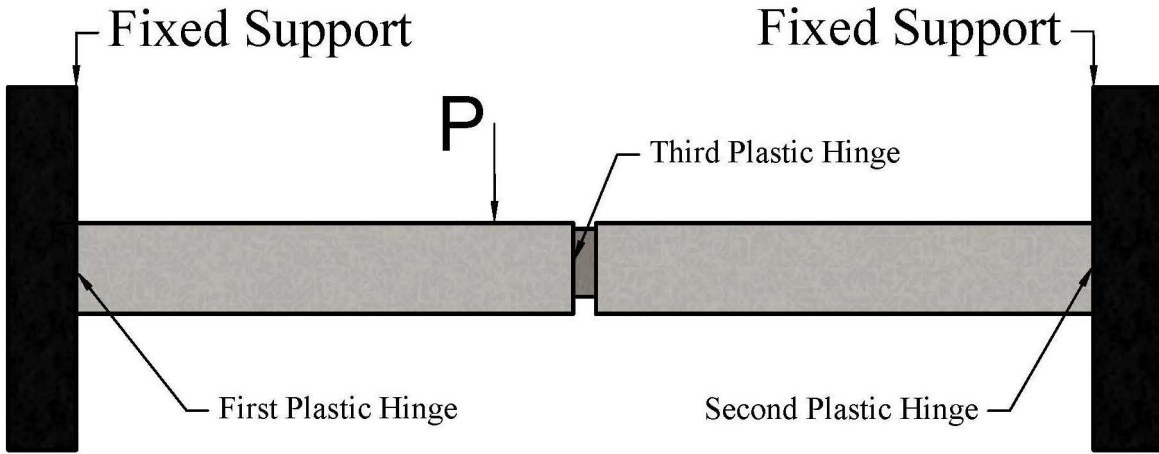


Figure 7.6. Flexural model plastic hinge location

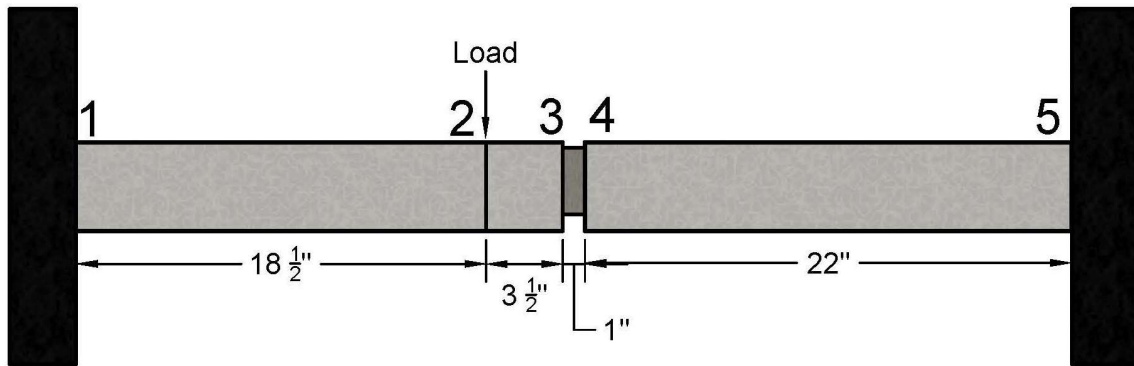


Figure 7.7. Half-width analysis detailing

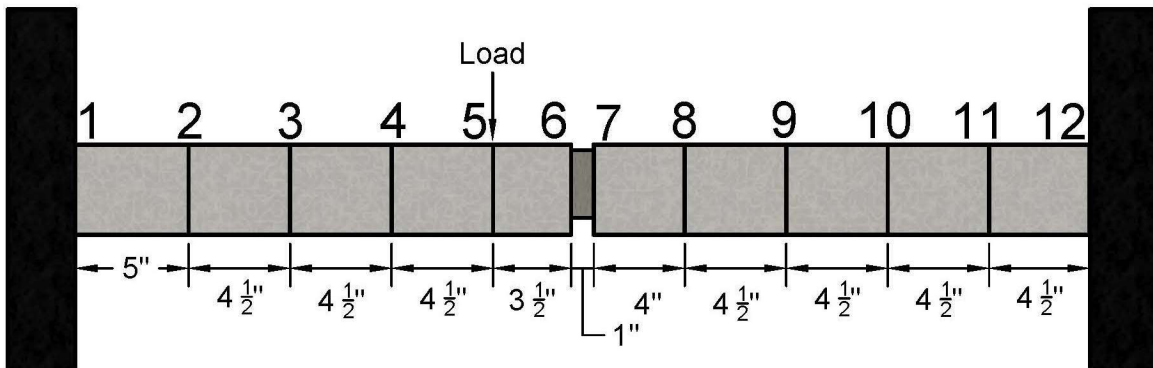


Figure 7.8. Tapered analysis side view detailing

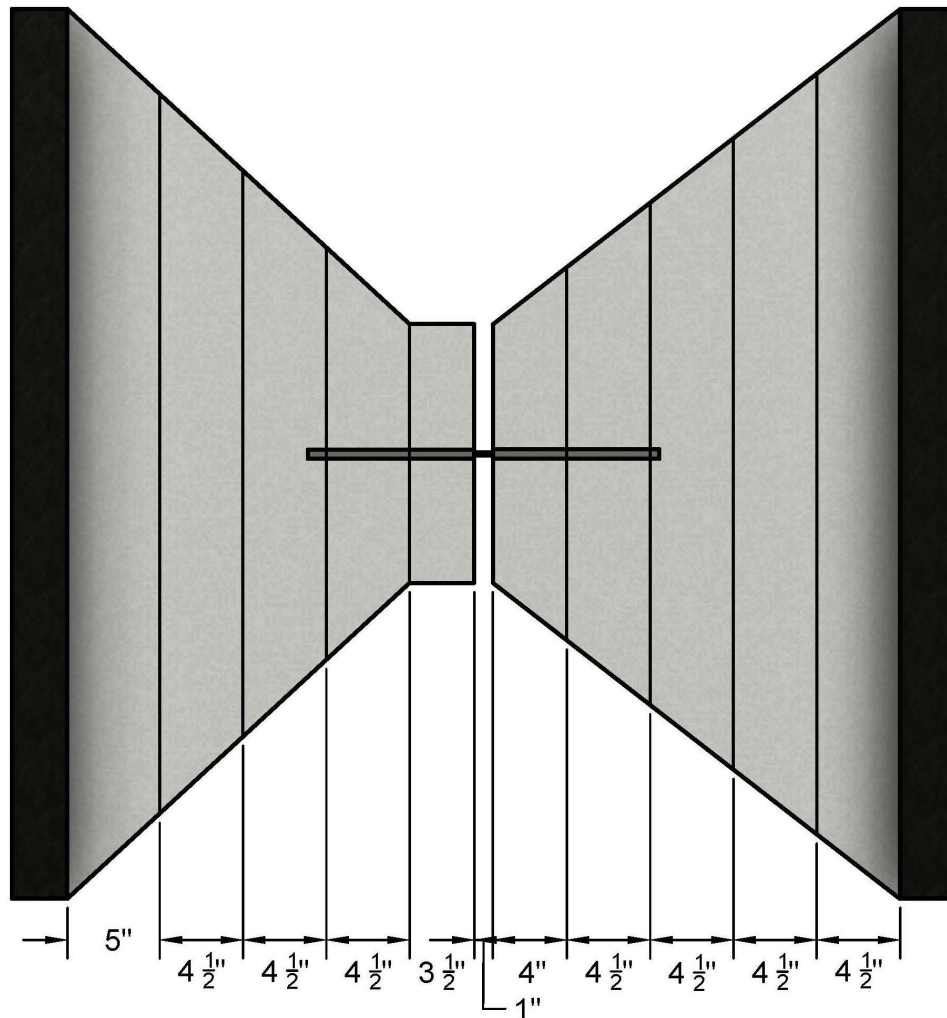


Figure 7.9. Tapered analysis top view detailing

The plastic hinges were assumed to form when the cantilevered spans cracked and began to rotate significantly about the edge of the table to which they were fixed. The stiffness of the model changed each time a plastic hinge is formed, which changed the boundary conditions of model as well. The loads and displacements are plotted on the flexural test results and is provided in Figure 7.10. The calculated results from the model are provided in Table 7.5, Table 7.6, and Table 7.7. The displacements generated from the model vary significantly from the experimental results. This error is expected to stem from the experimental measurements as the string potentiometer reading was taken from one side of the slab only, thus, the transverse tilting

of the slab was not captured experimentally. The results of the calculated loads were similar to those observed in the experiment. The calculated load at the third plastic hinge was only 38 pounds away from the peak load recorded in the experiment.

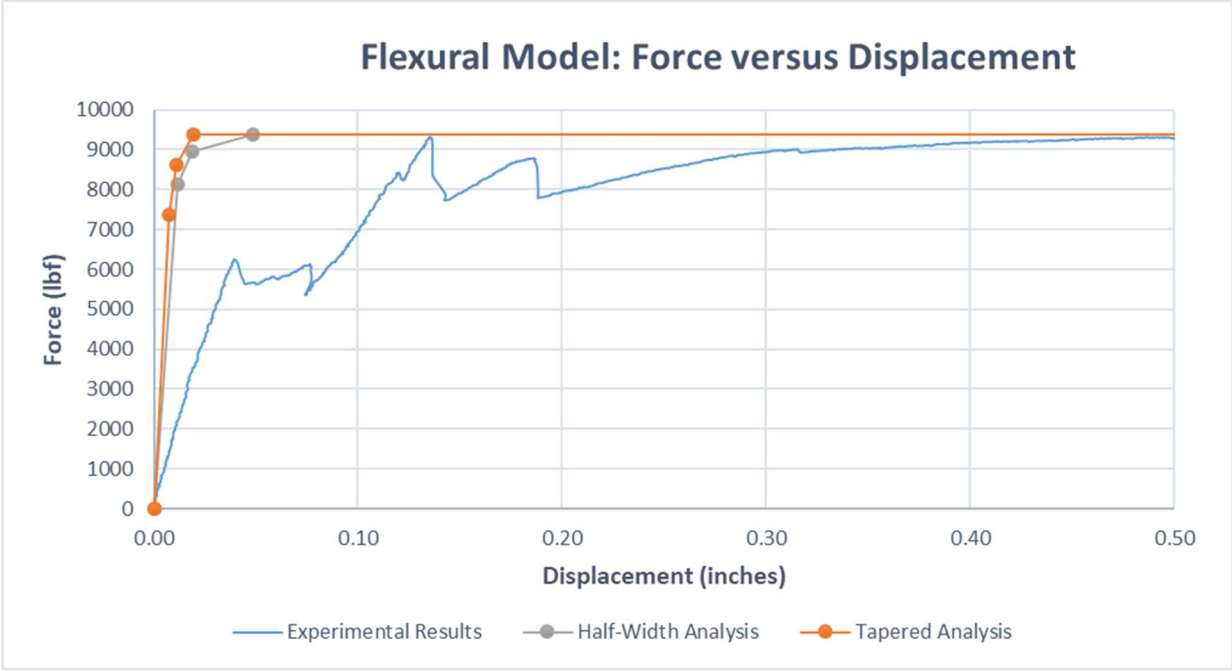


Figure 7.10. Flexural model load versus displacement plot

Table 7.5. First plastic hinge loads and displacements

Region	Force (lbf)	Displacement (inches)
Experimental 1 st Yield	6258	0.039
Tapered Analysis	7376	0.008
Half-Width Analysis	8131	0.012

Table 7.6. Second plastic hinge loads and displacements

Region	Force (lbf)	Displacement (inches)
Experimental 2 nd Yield	9333	0.135
Tapered Analysis	8628	0.011
Half-Width Analysis	8951	0.018

Table 7.7. Third plastic hinge loads and displacements

Region	Force (lbf)	Displacement (inches)
Experimental Peak	9329	0.487
Tapered Analysis	9367	0.019
Half-Width Analysis	9367	0.048

Chapter 8 - Conclusions and Recommendations

The proposed V-Wrap Stainless-Steel Shear Connector exhibited excellent behavior in both strength and ductility through experimental results from the tests conducted in this research. The use of the connector as an innovative repair method proved to be efficient and effective to strengthen preexisting structural elements. The ease of installation without the need of specialized equipment should be greatly considered by engineers when determining how to fix insufficient steel connections. The material composition of the connector will allow for an extended service life from the corrosion resistant properties and high yield strength of the stainless-steel.

The recorded data from the experimental program developed for the connector produced consistent results with similar failure modes in each of the tests. The monotonic loading protocol provided force-displacement stiffness relationships that were replicated with cyclic loading. The axial tension test provided two failure modes of concrete cracking in tension and debonding of the connector from the epoxy. The latter failure mode is believed to be associated with an unusual cold weather that the specimen was subjected to prior to testing. The monotonic and cyclic horizontal shear tests deformed the connectors significantly while maintaining capacity to carry a load. One monotonic horizontal shear test provided a failure mode that cracked the slab, but the failure mode occurred after a force over 20,000 lbf was applied to the connector. The monotonic and cyclic vertical shear tests observed a typical failure mode of concrete cracking in vertical shear, except for one test for each type of loading. The dissimilar vertical shear failure mode was when the concrete under the embedment of the connector cracked. This failure mode occurred from the presence of a gap between the slab and the testing table. The cyclic vertical shear test that broke through the bottom of the slab maintained a load due to the friction forces

between the connector and the epoxy. The flexural test observed yielding of both slabs and experienced significant deformation while a load similar to the ultimate load was maintained.

A strength capacity was determined from the average ultimate loads for each test type. The strength capacities were adjusted with a factor of safety of 3 and are provided in Table 8.1.

Table 8.1. Strength Capacity of the V-Wrap Stainless-Steel Shear connector

Test Type	Average Ultimate Force (lbf)	Strength Capacity (lbf)
Axial Tension Test	13220	4400
Monotonic Horizontal Shear Test	2575	850
Monotonic Vertical Shear Test	8393	2750
Cyclic Horizontal Shear Test	2900	950
Cyclic Vertical Shear Test	6681	2200
Flexural Test	9333	3100

Following the experimental tests performed in this research, here are some recommendations for future tests that could be conducted to further evaluate the strengths of the connector. Additional flexural tests should be conducted with various cyclic loading protocols. The recommended cyclic protocols are incremental steps of cyclic deformation, continuous cyclic loading, and alternated load cycles between the two slabs. The incremental cyclic deformation would be similar to the cyclic protocols conducted for the horizontal and vertical shear tests. The continuous cyclic loading would analyze fatigue responses of the connector for many load cycles. The alternated load cycles between the cantilevered slabs would simulate the loading of a vehicle passing over the connector, which would be a typical load sequence that occurs in parking garages. It is also recommended that a reverse cyclic loading protocol be conducted for the horizontal shear and vertical shear tests to investigate the strength of the

connector during seismic events that would cause moment reversals in a repaired system. Along with the need for additional tests, there were some observations made during the experimental tests that would improve the strength of the connector. The connector's transverse stiffness could be increased with the addition of a narrow flange to the top edge of the connector. The narrow flange would increase the lateral strength and stiffness against horizontal shearing forces by increasing the stiffness of the cross-section.

After the research outlined in this paper was conducted on the V-Wrap Stainless-Steel Shear Connector, it was concluded that the use of the proposed connector as a method to repair preexisting concrete elements to be adequate. The responses of the connector embedded in concrete slabs to simulate the behavior of the connector in the sides of double-tee concrete girders is particularly effective for the use in parking garage diaphragms.

References

1. Shaikh, A. F., & Feile, E. P. (2004). Load testing of a precast concrete double-tee flange connector. *PCI journal*, 49, 84-95.
2. Pincheira, J. A., Oliva, M. G., & Kusumo-Rahardjo, F. I. (1998). Tests on double tee flange connectors subjected to monotonic and cyclic loading. *PCI journal*, 43(3), 82-96.
3. Pincheira, J. A., Oliva, M. G., & Zheng, W. (2005). Behavior of double-tee flange connectors subjected to in-plane monotonic and reversed cyclic loads. *PCI journal*, 50(6), 32.
4. Van de Lindt, J. W. (2007). Experimental Behavior of Mechanical In-Flange Connectors. *The Open Civil Engineering Journal*, 1(1).
5. Naito, C. J., Cao, L., & Peter, W. (2009). Precast concrete double-tee connections, Part I: tension behavior. *PCI journal*, 54(1).
6. Cao, L., & Naito, C. (2009). Precast concrete double-tee connectors, part 2: Shear behavior. *PCI journal*, 54(2), 97.
7. Naito, C., & Ren, R. (2013). An evaluation method for precast concrete diaphragm connectors based on structural testing. *PCI journal*, 58(2).
8. Hendricks, R., Naito, C., & Osborn, A. (2018). Flange-to-flange double-tee connections subjected to vehicular loading, part 1: Numerical assessment approach. *PCI Journal*, 63(4), 41-53.
9. ACI Committee 318, American Concrete Institute, & ACI Committee 318. (2019). *Building code requirements for structural concrete (aci 318-19) : an aci standard*

; commentary on building code requirements for structural concrete (aci 318r-19).

American Concrete Institute.